**Gö-VIP-03: Prof. Dr. Holger Bastians**
Abteilung Molekulare Onkologie, UMG

***Originalpublikation**: "Increased microtubule assembly rates influence chromosomal instability in colorectal cancer." In: Nature Cell Biology. in press (DOI: 10.1038/ncb2994). Autoren: Norman Ertych (1), Ailine Stolz (1), Albrecht Stenzinger, Silke Kaulfuß, Peter Burfeind, Achim Aigner, Linda Wordeman & Holger Bastians (1)*

*(1) University Medical Center Goettingen (UMG) and Goettingen Center for Molecular Biosciences (GZMB), Institute of Molecular Oncology, Section for Cellular Oncology*

Die Publikation erschien am 29.6.2014 in Nature Cell Biology (online); in print: August Ausgabe Die beiden Erstautoren (NE, AS) und der Letzt/corresponding Autor (HB) sind Mitglieder der UMG und des GZMB

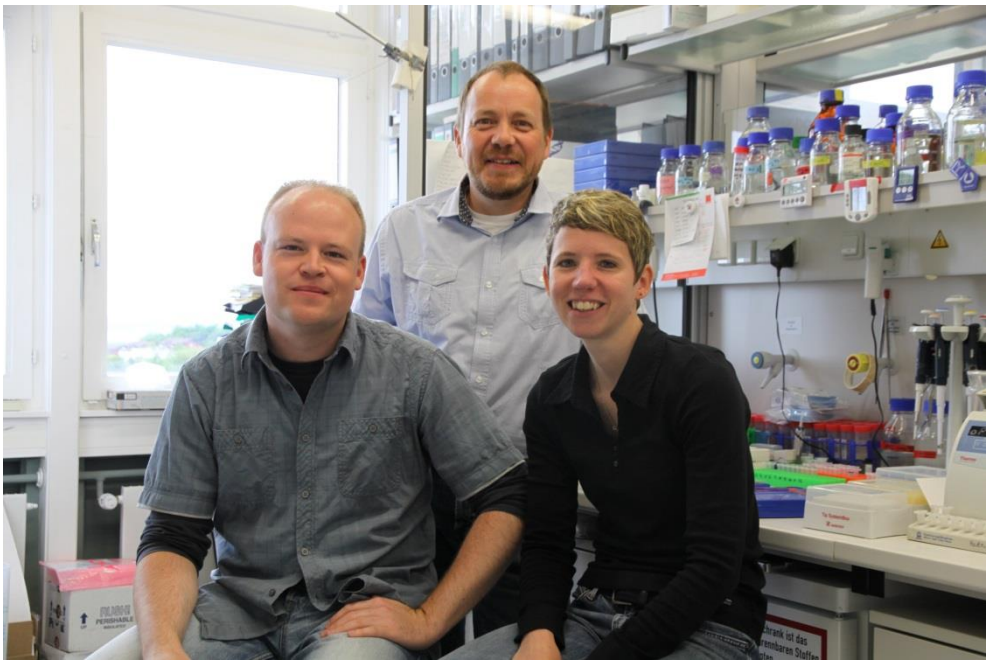

Abb.: Dr. Norman Ertych, Prof. Dr. Holger Bastians und Dr. Ailine Stolz (von links nach rechts)

**Zusammenfassung des wissenschaftlichen Inhalts**
**(Prof. Dr. Holger Bastians)**

Die chromosomale Instabilität (CIN) ist ein Haupt-Phänotyp von Tumorzellen und ist definiert als eine fortwährende Fehlverteilung von ganzen Chromosomen während der mitotischen Zellteilung. Dies führt zur Induktion und ständigen Veränderung von hochgradigen Aneuploidien in Krebszellen und stellt die Grundlage der genetischen Heterogenität und Wandelbarkeit in Tumorzellen dar. Es ist daher offensichtlich, dass der CIN-Phänotyp direkt die Adaption von Tumorzellen begünstigt und damit zur Tumorgenese, Tumorprogression und zur Entwicklung von Therapieresistenzen beitragen kann. Obwohl Chromosomen-Fehlverteilungen und Aneuploidie ist fast allen soliden Tumoren nachweisbar sind und dies bereits vor über 100 Jahren vom deutschen Zellbiologen Theodor Boveri erstmals als ein Krebs-assoziierter Phänotyp beschrieben wurde, sind die molekularen Grundlagen der Chromosomenfehlverteilung in Krebszellen bisher weitgehend unklar.

In unserer jüngsten Arbeit haben wir nun erstmals gezeigt, dass Veränderungen in der Mikrotubuli-Dynamik in mitotischen Spindeln nicht nur sehr häufig in chromosomal instabilen Krebszellen nachweisbar sind, sondern auch auslösend für den CIN-Phänotyp und für Erzeugung von Aneuploidien sein können. In Lebendzell-Mikroskopie Experimenten haben wir in solchen Tumorzellen, die sich durch den CIN-Phänotyp auszeichnen, eine Erhöhung der Mikrotubuli-Wachstumsraten an deren Plusenden nachgewiesen. Dies hat eine transiente Fehl-Orientierung der mitotischen Spindel zur Folge, was schließlich zu fehlerhaften Anheftungen der Kinetochoren an die mitotischen Spindel-Mikrotubuli und zu Chromosomen-Fehlverteilungen während der Anaphase der Mitose führt.

Wir haben mit CHK2 und BRCA1 zwei wichtige Tumorsuppressorgene und mit AURORA-A ein zentrales Onkogen identifiziert, deren Verlust bzw, Überexpression in Tumoren sehr häufig zu detektieren ist und eine Erhöhung der Mikrotubuli-Wachstumsraten zur Folge hat. Dieses Netzwerk aus Tumorsuppressoren und Onkogen reguliert offenbar eine Mikrotubuli-Polymerase, deren erhöhte Aktivität in Tumorzellen zu einer Erhöhung der Mikrotubuli-Dynamik führt. Konsequenterweise konnten wir die erhöhte Mikrotubuli-Dynamik entweder durch eine partielle Hemmung der onkogene Aktivität von Aurora-A oder der Mikrotubuli-Polymerase unterdrücken. Dies war ebenso möglich durch die Anwendung von sehr geringen Dosen von Taxol, einem Mikrotubuli-bindenden Chemotherapeutikum, das schon lange für die anti-Tumor Therapie eingesetzt wird. Diese verschiedenen Strategien führten in der Tat zu einer Unterdrückung des CIN-Phänotyps in verschiedenen Krebszellen, was den auslösenden Charakter der Erhöhung der Mikrotubuli-Dynamik für die Chromosomen-Fehlverteilungen bestätigt.

Damit hat unsere Studie nicht nur einen in Tumorzellen hochrelevanten Mechanismus zur Erzeugung des CIN-Phänotyps aufgezeigt, sondern ist auch die Grundlage, diesen zentralen Tumor-Phänotyp, der mit einer schlechten Prognose und Therapie-Resistenz assoziiert ist, zu unterdrücken. Unsere zukünftigen Arbeiten werden nun untersuchen, ob die gezielten Hemmung des CIN-Phänotyps als eine neue weitgreifende Therapie-Option für Tumoren mit dem CIN-Phänotyp eingesetzt werden kann, um möglicherweise die Entstehung von Therapie-Resistenzen zu unterdrücken.

**WEITERE INFORMATIONEN:**

Prof. Dr. Holger Bastians
Einrichtung: Molekulare Onkologie
Telefon: 0551-39-33823
E-Mail: holger.bastians@uni-goettingen.de

**Weitere Links:**

- PubMed
- Presseinformation Nr. 098 vom 02. Juli 2014 - "Wie Tumore sich anpassen"

nature cell biology

# Increased microtubule assembly rates influence chromosomal instability in colorectal cancer cells

Norman Ertych[1,7], Ailine Stolz[1,7], Albrecht Stenzinger[2], Wilko Weichert[2,3], Silke Kaulfuß[4], Peter Burfeind[4], Achim Aigner[5], Linda Wordeman[6] and Holger Bastians[1,8]

**Chromosomal instability (CIN) is defined as the perpetual missegregation of whole chromosomes during mitosis and represents a hallmark of human cancer. However, the mechanisms influencing CIN and its consequences on tumour growth are largely unknown. We identified an increase in microtubule plus-end assembly rates as a mechanism influencing CIN in colorectal cancer cells. This phenotype is induced by overexpression of the oncogene *AURKA* or by loss of the tumour suppressor gene *CHK2*, a genetic constitution found in 73% of human colorectal cancers. Increased microtubule assembly rates are associated with transient abnormalities in mitotic spindle geometry promoting the generation of lagging chromosomes and influencing CIN. Reconstitution of proper microtubule assembly rates by chemical or genetic means suppresses CIN and thereby, unexpectedly, accelerates tumour growth *in vitro* and *in vivo*. Thus, we identify a fundamental mechanism influencing CIN in cancer cells and reveal its adverse consequence on tumour growth.**

Colorectal cancer (CRC) represents a prime example of a tumour entity exhibiting CIN, which is thought to contribute to tumorigenesis, tumour progression and therapy resistance[1–4]. However, despite being such an important phenotype, the causes leading to and the direct consequences resulting from CIN are poorly understood. Several mechanisms including a weakened spindle checkpoint, chromatid cohesion defects and also replication stress have been proposed to contribute to CIN, but none of these mechanisms can account for the widespread appearance of CIN in human cancer[4–6]. However, a major pre-stage of chromosome missegregation in cancer cells are so-called lagging chromosomes, which are the consequence of erroneous attachments of a single kinetochore to microtubules emanating from opposing spindle poles[7,8]. In general, those erroneous kinetochore attachments also occur stochastically in the early phases of a normal mitosis, but are usually corrected before anaphase onset[8]. However, the details of this correction process are not well understood[8–12] and it seems that kinetochore attachment error correction is rarely inactivated in human cancer. It is, however, conceivable that increased rates of kinetochore–microtubule mal attachments might overwhelm the capacity of the cellular error correction machinery. Indeed, this has been demonstrated for a subset of cancer cells exhibiting supernumerary centrosomes. In these cases, transient multipolar spindle intermediates can facilitate the generation of erroneous kinetochore attachments and, thus, promote the generation of lagging chromosomes despite the presence of error correction[13,14]. However, because most cancer cells do not exhibit supernumerary centrosomes[15], additional, yet unknown mechanisms promoting the generation of lagging chromosomes are likely to exist. Interestingly, in human cancer cells a number of established oncogenes and tumour suppressor genes are implicated in proper mitotic chromosome segregation[16]. For instance, PLK1 and aurora-A are centrosomal kinases involved in mitotic spindle assembly[17], but the consequences resulting from their overexpression, which is often detected in human cancer cells[18,19], are unclear. Similarly, previous publications have reported on a requirement of the tumour suppressors *CHK2* and *BRCA1* for normal mitotic chromosome segregation[20,21]. The mechanism of how the overexpression of these oncogenes or the loss of these tumour suppressor genes causes CIN remains an open question.

## RESULTS

### Increased mitotic microtubule plus-end assembly rates are characteristic for CRC cells exhibiting CIN

We addressed the role of microtubule assembly dynamics within mitotic spindles as a possible and yet unexplored mechanism that

[1]Institute of Molecular Oncology, Section for Cellular Oncology, Goettingen Center for Molecular Biosciences (GZMB) and University Medical Center, Georg-August University, D-37077 Goettingen, Germany. [2]Institute for Pathology, University Medical Center, Ruprecht-Karls-University, D-69120 Heidelberg, Germany. [3]German Consortium for Translational Cancer Research, D-69120 Heidelberg, Germany. [4]Institute for Human Genetics, University Medical Center, Georg-August University, D-37073 Goettingen, Germany. [5]Rudolf-Boehm-Institute for Pharmacology and Toxicology, Clinical Pharmacology, University of Leipzig, D-04107 Leipzig, Germany. [6]Department of Physiology and Biophysics, University of Washington, School of Medicine, Seattle, Washington 98195, USA. [7]These authors contributed equally to this work.
[8]Correspondence should be addressed to H.B. (e-mail: holger.bastians@uni-goettingen.de)

Received 3 March 2014; accepted 20 May 2014; published online 29 July 2014; DOI: 10.1038/ncb2994

could influence CIN in human cancer cells. To this end, we measured microtubule plus-end assembly rates in live cells during mitosis by tracking the microtubule end-binding protein EB3 fused to GFP (ref. 22). We used a panel of CRC cells, which can be categorized into chromosomally stable MIN/MSI cell lines with a near-diploid karyotype (HCT116, SW48 and RKO) and cell lines exhibiting CIN (SW837, LS1034, SW620, SW480, HT29 and CaCo-2). To ensure comparable measurements of the various cell lines, we synchronized cells in mitosis by using the small-molecule inhibitor dimethylenastron[23] (DME) targeting the mitotic kinesin Eg5 (also known as Kif11), which resulted in the formation of monopolar spindles[24]. Neither this synchronization step nor the expression level of EB3–GFP influenced microtubule plus-end assembly rates (Supplementary Figs 1a,b and 2e). Intriguingly, we found that all CIN cell lines exhibited significantly increased microtubule assembly rates when compared with MIN/MSI cell lines or with non-transformed human RPE-1 cells (Fig. 1a) suggesting that abnormal microtubule plus-end assembly rates might be linked to CIN.

### Increased mitotic microtubule plus-end assembly rates influence CIN

To investigate the relationship between increased microtubule assembly rates and CIN we restored normal microtubule assembly rates in CIN cells by partially lowering the expression of the microtubule polymerase ch-TOG (also known as CKAP5; Supplementary Fig. 1c), which mediates the assembly of $\alpha_v\beta$-tubulin subunits at microtubule plus ends[25,26]. Live-cell analyses of stable cell lines demonstrated that partial repression of *CH-TOG* was sufficient to restore normal microtubule assembly rates in CIN cells to a level typically seen in chromosomally stable cells (Fig. 1b). Partial repression of *CH-TOG* does not affect normal cell cycle progression or cell viability (Supplementary Fig. 3d). Most importantly, karyotype analyses using chromosome counting and interphase fluorescence *in situ* hybridization revealed a significant reduction of karyotype variability and, thus, of CIN after restoration of normal microtubule plus-end assembly rates (Fig. 1c and Supplementary Fig. 1d and Table 1). These results indicate that increased microtubule plus-end assembly rates can influence CIN in cancer cells.

### Drug-mediated alterations in mitotic microtubule plus-end assembly rates affect karyotype stability

As another independent approach to restore normal microtubule assembly rates in CIN cells we used Taxol, a microtubule-binding drug known to suppress microtubule assembly, preferentially at the plus ends[27–29]. We identified sub-nanomolar concentrations of Taxol that were sufficient to suppress the increased microtubule assembly rates in different CIN cell lines without affecting cell viability or normal cell cycle progression (Fig. 1d,e and Supplementary Fig. 1e). Most strikingly, low-dose Taxol treatment significantly suppressed CIN (Fig. 1f and Supplementary Fig. 1f and Table 1). Remarkably, removal of Taxol re-induced increased microtubule plus-end assembly rates and CIN in the same single-cell clones (Fig. 1e,f and Supplementary Table 1). In addition, we used sub-nanomolar concentrations of nocodazole, a microtubule-binding drug known to have opposite effects on microtubule dynamics compared with Taxol[30], and detected an increase in microtubule assembly rates and an induction of CIN in otherwise chromosomally stable HCT116 cells (Fig. 1h and Supplementary Table 1). Together, these results indicate that subtle alterations in microtubule plus-end assembly rates are sufficient to affect the numerical karyotype stability in cancer cells.

### Overexpression of the oncogene *AURKA* or loss of the tumour suppressor gene *CHK2* influences CIN by increasing mitotic microtubule assembly rates

To identify cancer-relevant genetic lesions that confer increased microtubule assembly rates we investigated the role of the most frequent genetic alterations found in CRC (summarized in Supplementary Fig. 2a) previously implicated in mitotic processes[18,19,31–35]. Live-cell analyses of cells engineered to harbour these different genetic alterations (Supplementary Fig. 2b) showed that the overexpression of *AURKA* or loss of *CHK2* increased microtubule assembly rates to a level typically found in chromosomally unstable CRC cell lines (Fig. 2a). Moreover, single-cell clones derived from stable cell lines exhibiting these genetic lesions evolved a high karyotype variability and, thus, CIN (Fig. 2b–d and Supplementary Fig. 2b–e and Table 1). However, the increase in microtubule assembly rates was neither associated with supernumerary centrosomes (Supplementary Fig. 2f) nor with overt changes in other microtubule dynamics parameters such as overall dynamicity, frequency of catastrophe events or time spent paused (Supplementary Fig. 2g–i). Importantly, restoration of normal microtubule plus-end assembly rates mediated by a partial repression of *CH-TOG* (Fig. 2b,c and Supplementary Fig. 3a,b) or by treatment with sub-nanomolar doses of Taxol (Fig. 2e,f) resulted in a significant suppression of CIN (Fig. 2d,g and Supplementary Fig. 3c–e and Table 1). Thus, we demonstrate that overexpression of the oncogene *AURKA* or loss of the tumour suppressor gene *CHK2* increases microtubule assembly and influences CIN in CRC cells.

### Increased microtubule assembly rates are associated with transient mitotic spindle geometry defects

To investigate the link between increased microtubule assembly rates and chromosome missegregation we analysed the structure of mitotic spindles in cell lines overexpressing *AURKA* or deficient for *CHK2*. Interestingly, in both cases we found very similar abnormal mitotic spindle structures, which were suppressed on restoration of normal microtubule assembly rates by partial repression of *CH-TOG* (Fig. 3a–c). Further live-cell microscopy analyses revealed that the spindle structure abnormalities were transient and associated with a timely delay in chromosome alignment (see examples in Supplementary Videos 1 and 2). Importantly, those cells eventually achieved full alignment of chromosomes and initiated anaphase, albeit at the expense of chromosome missegregation. The transient nature of spindle abnormalities in those cells prompted us to analyse the dynamic positioning of the spindle axes by detecting GFP–centrin as a marker for centrosomes in live cells (Fig. 3d). In fact, during late prometaphase when the distance of the two centrosomes was maximal (Supplementary Videos 3 and 4) we found significantly increased angles of spindle axes and, thus, a misalignment of the mitotic spindle in cells exhibiting increased microtubule assembly rates (Fig. 3e). This spindle mispositioning seen in live cells was no longer apparent in metaphase (Fig. 3e), supporting our initial

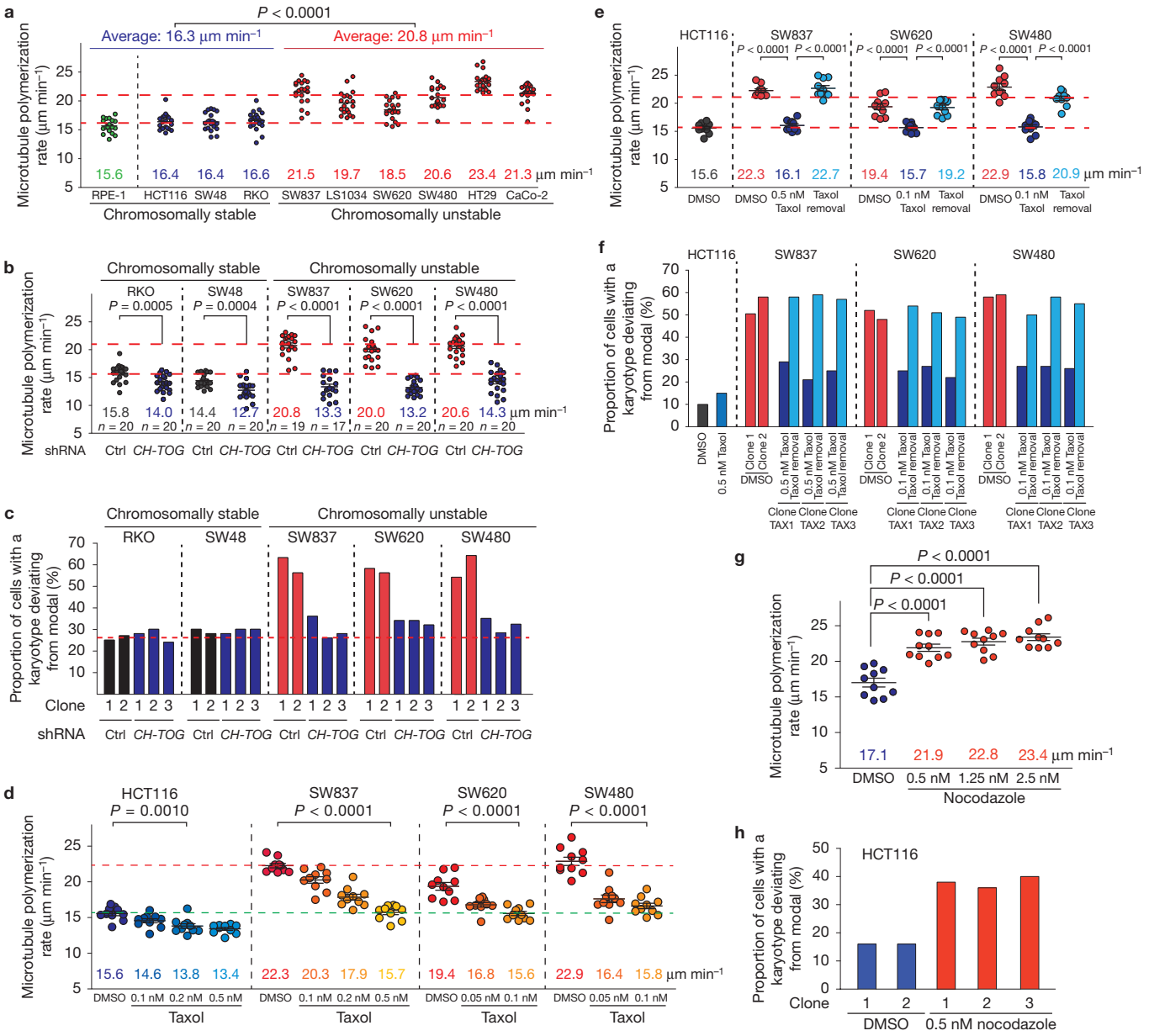


**Figure 1** Increased mitotic microtubule assembly rates are a common characteristic of chromosomally unstable CRC cells and mediate numerical chromosome instability. (**a**) Measurement of mitotic microtubule plus-end assembly rates in various CRC cell lines. Scatter dot plots show average assembly rates based on measurements of 20 microtubules per cell (mean ± s.e.m., *t*-test, $n = 20$ cells from three independent experiments). (**b**) Measurement of mitotic microtubule plus-end assembly rates in stable CRC cell lines expressing control shRNA or shRNAs targeting *CH-TOG*. Scatter dot plots show average assembly rates (20 microtubules per cell, mean ± s.e.m., *t*-test, $n = 17$–$20$ cells from three independent experiments). (**c**) Determination of chromosome number variability of single-cell clones shown in **b**. The proportion of cells showing chromosome numbers deviating from the modal were determined after 30 generations (50–103 cells analysed for each condition). (**d**) Measurement of mitotic microtubule plus-end assembly rates after titration of sub-nanomolar doses of Taxol. Scatter dot plots show average assembly rates (20 microtubules per cell, mean ± s.e.m., *t*-test, $n = 10$ cells from three independent experiments). (**e**) Measurement of mitotic microtubule plus-end assembly rates of single-cell clones derived from CRC cell lines and grown in the absence or presence of low doses of Taxol or after subsequent removal of Taxol. Scatter dot plots show average assembly rates (20 microtubules per cell, mean ± s.e.m., *t*-test, $n = 10$ cells from three independent experiments). (**f**) Determination of chromosome number variability in single-cell clones generated as in **e**. The proportion of cells showing chromosome number deviations from the modal were determined after 30 generations (100–109 cells analysed for each condition). Three independent single cell clones grown in the presence of Taxol (TAX1, 2 and 3) were analysed. (**g**) Measurements of mitotic microtubule plus-end assembly rates in chromosomally stable HCT116 cells after treatment with low doses of nocodazole. Scatter dot plots show average assembly rates (20 microtubules per cell, mean ± s.e.m., *t*-test, $n = 10$ cells from three independent experiments). (**h**) Determination of chromosome number variability in single-cell clones generated in the absence or presence of low-dose nocodazole. The proportion of cells showing chromosome number deviations from the modal were determined after 30 generations (50 cells per condition). Detailed data on karyotype analyses can be found in Supplementary Table 1. Statistic source data for Fig. 1 can be found in Supplementary Table 2.

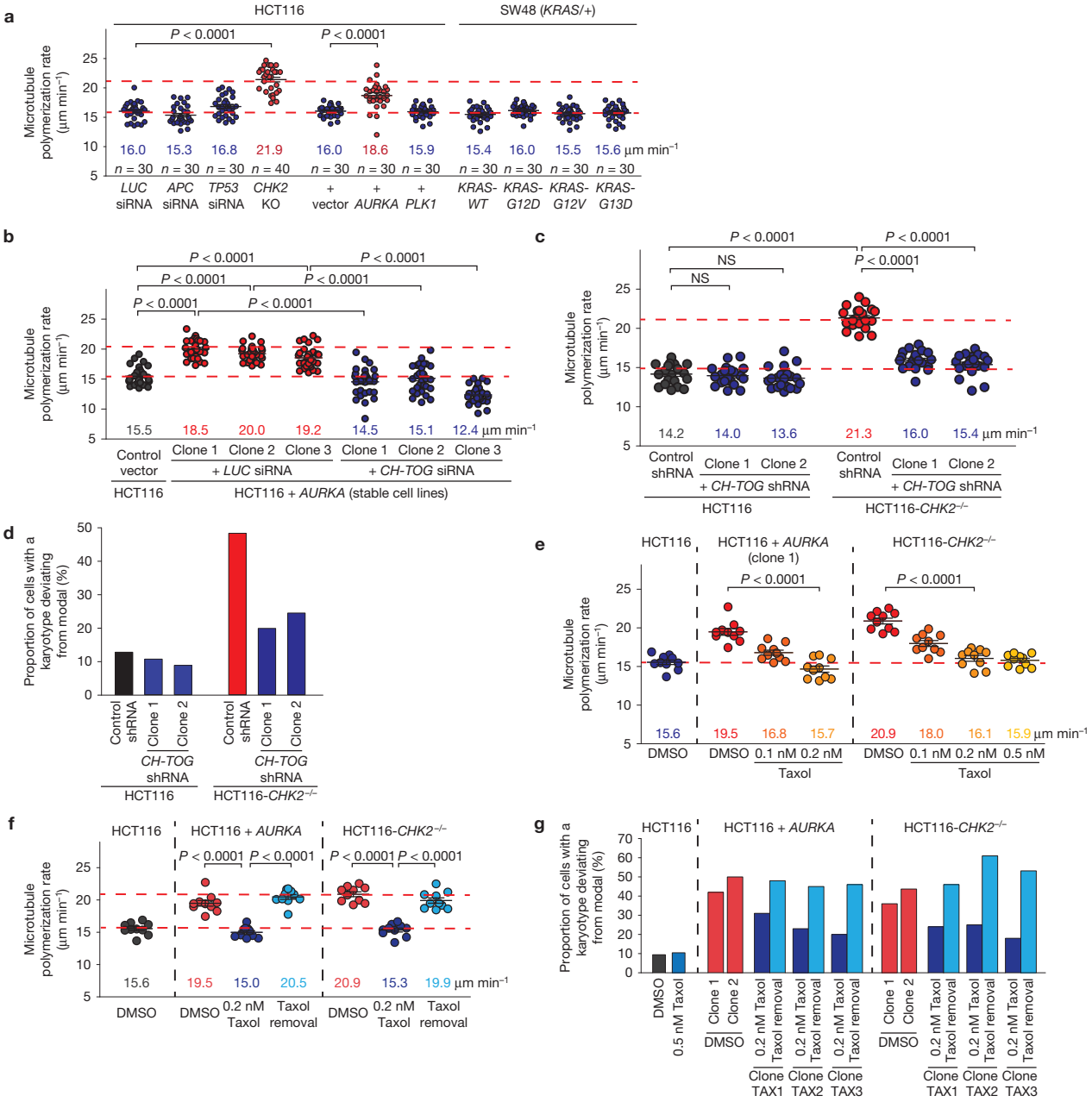


**Figure 2** Identification of *AURKA* overexpression and *CHK2* loss as genetic lesions triggering increased microtubule assembly rates in CRC cells. (**a**) Measurement of mitotic microtubule plus-end assembly rates in HCT116 cells harboring the indicated genetic alterations. Scatter dot plots show average assembly rates (20 microtubules per cell, mean ± s.e.m., *t*-test, $n=30$–40 cells from three independent experiments). (**b**) Measurement of mitotic microtubule plus-end assembly rates in cells stably overexpressing *AURKA* and transfected with control or *CH-TOG* siRNAs. Scatter dot plots show average assembly rates based on measurements of 20 microtubules per cell (mean ± s.e.m., *t*-test, $n=30$ cells from three independent experiments). (**c**) Measurement of mitotic microtubule plus-end assembly rates in *CHK2*-deficient cells stably transfected with shRNAs targeting *CH-TOG*. Scatter dot plots show average assembly rates based on measurements of 20 microtubules per cell (mean ± s.e.m., *t*-test, $n=20$ cells from three independent experiments). NS, not significant. (**d**) Karyotype analyses of single-cell clones derived from HCT116 and HCT116-*CHK2*$^{-/-}$ stably repressing *CH-TOG*. The proportion of cells showing chromosome number deviations from the modal were determined after 30 generations (50 cells per condition). (**e**) Measurement of mitotic microtubule plus-end assembly rates of HCT116 cells overexpressing *AURKA* or deficient for *CHK2* after titration of sub-nanomolar doses of Taxol. Scatter dot plots show average assembly rates (20 microtubules per cell, mean ± s.e.m., *t*-test, $n=10$ cells from three independent experiments). (**f**) Measurement of mitotic microtubule plus-end assembly rates in single-cell clones derived from HCT116 cells stably overexpressing *AURKA* or deficient for *CHK2* and grown in the absence, presence or after removal of low-dose Taxol. Scatter dot plots show average growth rates (20 microtubules per cell, mean ± s.e.m., *t*-test, $n=10$ cells from three independent experiments). (**g**) Determination of chromosome number variability in single-cell clones shown in **f**. The proportion of cells showing chromosome numbers deviating from the modal were determined (100–103 cells per condition). Three independent single cell clones grown in the presence of Taxol (TAX1, 2 and 3) were analysed. Three independent single cell clones grown in the presence of Taxol (TAX1, 2 and 3) were analysed. Detailed data on karyotype analyses can be found in Supplementary Table 1. Statistic source data for Fig. 2 can be found in Supplementary Table 2.

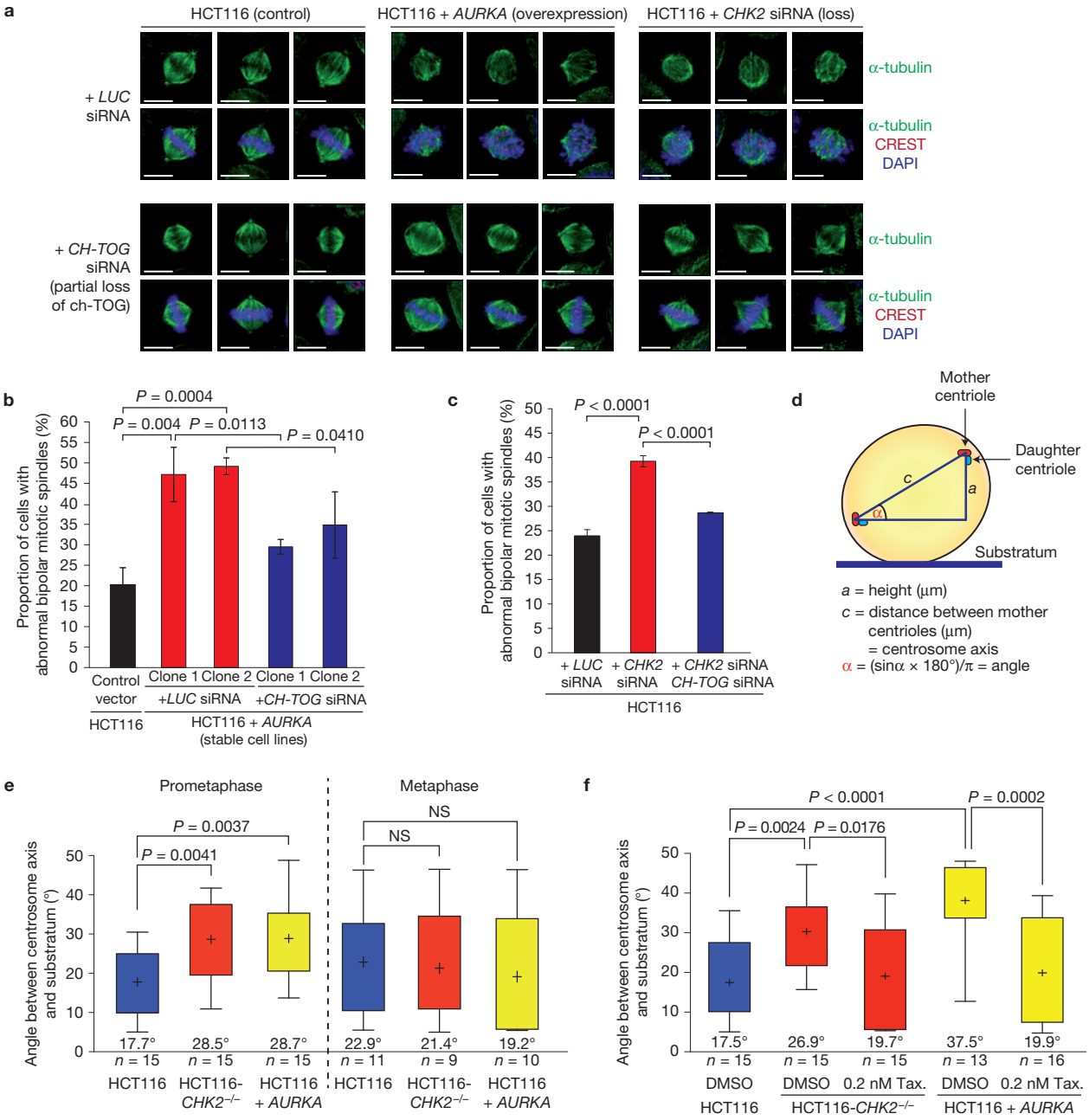


**Figure 3** Increased microtubule assembly rates result in abnormal mitotic spindle geometry. (**a**) Representative examples of metaphase spindle structures from cells overexpressing *AURKA* or deficient for *CHK2* with or without partial repression of *CH-TOG* (CREST marks kinetochores; scale bars, 10 μm). (**b**) Quantification of abnormal bipolar metaphase spindle structures in HCT116 cells stably overexpressing *AURKA* before and after partial depletion of *CH-TOG*. The graphs show mean values ± s.d., *t*-test ($n = 3$ independent experiments with a total of 240–1,100 mitotic cells evaluated). (**c**) Quantification of abnormal bipolar metaphase spindle structures in HCT116 cells after depletion of *CHK2* and after concomitant repression of *CH-TOG*. The graphs show mean values ± s.d., *t*-test ($n = 3$ independent experiments with a total of 1,000–1,300 mitotic cells evaluated). (**d**) Schematic depiction of the experimental measurement of spindle axes positioning. (**e**) Determination of angles of the spindle axes in cells overexpressing *AURKA* or deficient for *CHK2* in prometaphase and metaphase cells. The box and whisker plots show the range, mean and quartile of the measurements (*t*-test, $n = 9$–15 cells from three independent experiments). NS, not significant. (**f**) Determination of angles of the spindle axes in prometaphase cells before and after reconstitution of normal microtubule assembly rates by low-dose Taxol treatment. The box and whisker plot shows the range, mean and quartile of the measurements (*t*-test, $n = 13$–16 cells from three independent experiments). Statistic source data for Fig. 3 can be found in Supplementary Table 2.

observation of transient spindle geometry abnormalities in fixed cells. Remarkably, restoration of normal microtubule assembly rates by low-dose Taxol treatment suppressed the spindle mispositioning (Fig. 3f), indicating that an increase in microtubule assembly rates can influence transient spindle geometry abnormalities during the early phases of mitosis.

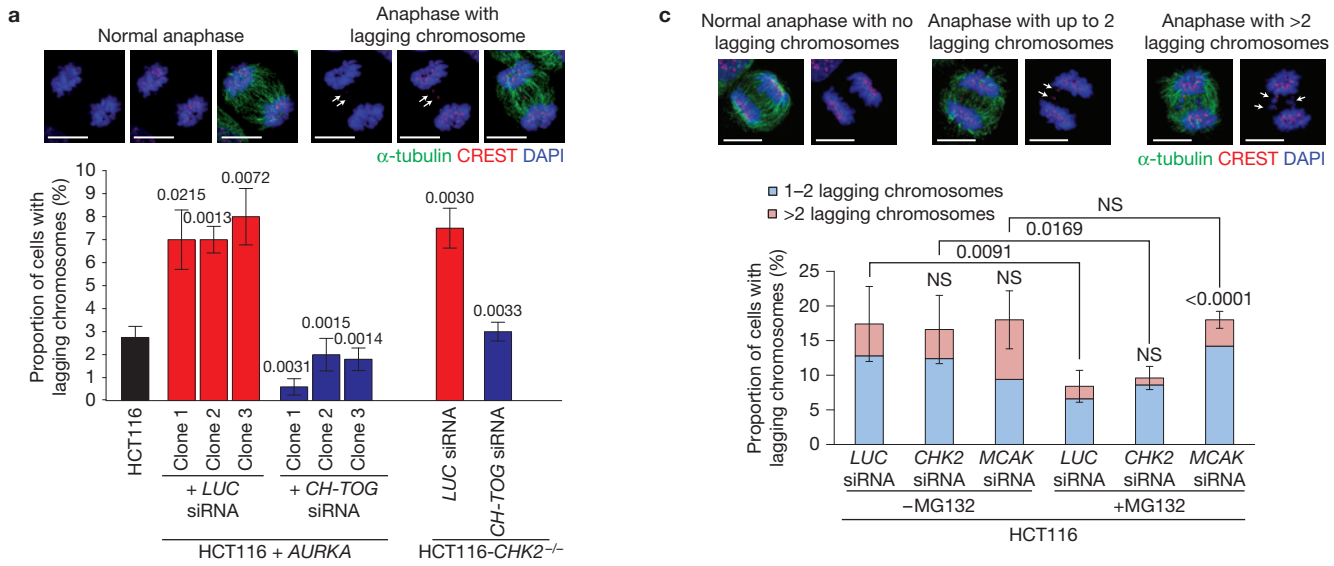


**b**

| | Kinetochore–microtubule turnover (average ± s.e.m.) | | |
|---|---|---|---|
| | $T_{1/2}$ (min) | $R^2$ | *n* |
| HCT116 + control vector | 1.23 ± 0.22 | 0.9246 | 23 |
| HCT116 + *AURKA* (clone 1) | 2.38 ± 0.43 | 0.8948 | 36 |
| HCT116 + *AURKA* (clone 2) | 2.38 ± 0.30 | 0.9487 | 27 |
| HCT116 (parental) | 1.23 ± 0.05 | 0.9926 | 9 |
| HCT116-*CHK2*$^{-/-}$ + DMSO | 2.35 ± 0.13 | 0.9947 | 13 |
| HCT116-*CHK2*$^{-/-}$ + 0.2 nM Taxol | 1.93 ± 0.13 | 0.9297 | 14 |

**d**

| | Kinetochore–microtubule turnover (average ± s.e.m.) | | |
|---|---|---|---|
| | $T_{1/2}$ (min) | $R^2$ | *n* |
| HCT116: monastrol washout, early | 3.28 ± 0.02 | 0.9907 | 22 |
| HCT116: monastrol washout, late | 1.50 ± 0.05 | 0.9860 | 14 |

**Figure 4** Increased microtubule assembly rates promote the generation of lagging chromosomes without interfering with error correction. (**a**) Quantification of the proportion of cells exhibiting lagging chromosomes using HCT116 cells overexpressing *AURKA* or deficient for *CHK2* and transfected with siRNAs targeting *CH-TOG*. Representative examples are given (scale bars, 10 μm). The graph shows mean values ± s.e.m. (*t*-test, $n = 4$ independent experiments with a total number of 230–350 anaphase cells evaluated). (**b**) Summary of kinetochore–microtubule turnover measurements in the indicated cell lines expressing photoactivatable GFP–tubulin (PA-GFP–tubulin). The addition of low concentrations of Taxol suppressed the observed hyper-stabilization of kinetochore–microtubule attachments in *CHK2*-deficient cells (average ± s.e.m., $n = 9$–36 cells from three independent experiments). (**c**) Quantification of the proportion of HCT116 cells showing lagging chromosomes after washout of monastrol and prolonging metaphase by MG132 treatment in the presence or absence of CHK2 or MCAK. Representative examples are given (scale bars, 10 μm). The graph shows mean values ± s.d. for cells exhibiting 1–2 and more than 2 lagging chromosomes per anaphase (*t*-test, $n = 5$ independent experiments with a total of 500 anaphase cells evaluated). NS, not significant. (**d**) Summary of kinetochore–microtubule turnover measurements in HCT116 cells expressing PA-GFP–tubulin immediately after establishing bipolar spindles on release from a monastrol block (early) and after release from monastrol into MG132 to prolong time for error correction (late). The table shows average ± s.e.m., $n = 14$–22 cells from three independent experiments. Statistic source data for Fig. 4 can be found in Supplementary Table 2.

### Increased microtubule plus-end assembly rates promote the generation of lagging chromosomes without interfering with error correction

We investigated whether an increase in microtubule assembly associated with transient spindle geometry abnormalities might represent a cancer-relevant mechanism for the generation of lagging chromosomes. Indeed, the number of lagging chromosomes during anaphase was significantly increased in cells with increased microtubule assembly rates and suppressed when normal microtubule assembly rates were restored (Fig. 4a). As lagging chromosomes can result from an impairment of error correction that is associated with increased microtubule–kinetochore attachment stability[8,10,36,37], we determined the microtubule–kinetochore attachment stability by measuring microtubule turnover in live cells (Supplementary Fig. 4a–c). Intriguingly, we found hyper-stable microtubule–kinetochore attachments in cells with increased microtubule assembly rates, which were suppressed by restoration of proper microtubule assembly (Fig. 4b). To test the possibility that increased microtubule assembly rates might interfere with error correction, we induced erroneous kinetochore attachments by a monastrol washout procedure, followed by a release of these cells into medium containing the proteasome inhibitor MG132 to provide extra time for error correction by prolonging metaphase as shown previously[38]. Importantly, cells with increased microtubule assembly rates were

able to efficiently reduce the number of lagging chromosomes during anaphase, whereas *MCAK*-depleted cells, which are impaired in error correction[9–12], showed the persistence of lagging chromosomes even after prolonging the time for error correction (Fig. 4c and Supplementary Fig. 4d). Hence, despite the presence of hyper-stable microtubule–kinetochore attachments, the increase in microtubule plus-end assembly rates as an influencing factor for CIN does not interfere with error correction. Vice versa, both depletion of *MCAK* or *APC*, which reduces the turnover of kinetochore–microtubules[10,37], or overexpression of *MCAK* in CIN cells, which promotes error correction[10], caused no alteration in microtubule plus-end assembly rates (Supplementary Fig. 4e–h). Thus, increased microtubule assembly rates and impaired error correction, both of which lead to lagging chromosomes and CIN, seem to be separable mechanisms. As both conditions are associated with hyper-stable microtubule–kinetochore attachments we examined whether this might be associated with erroneous kinetochore attachments *per se*. To test this, we analysed kinetochore–microtubule turnover in chromosomally stable HCT116 cells after release from a monastrol block in the presence or absence of MG132. Although the microtubule assembly rates were not changed (Supplementary Fig. 4i), the half-life of kinetochore–microtubules in bipolar spindles was significantly increased on induction of erroneous attachments and clearly suppressed after extended error correction (Fig. 4d and Supplementary Fig. 4j), suggesting that erroneous attachments might be associated with a higher stability *per se*. Thus, we conclude that increased microtubule assembly rates and impairment of error correction are separable mechanisms, both of which are associated with hyper-stability of erroneous microtubule–kinetochore attachments leading to the generation of lagging chromosomes.

### The *CHK2–BRCA1* tumour suppressor pathway negatively regulates the oncogene *AURKA* to ensure proper microtubule assembly rates

To investigate the cancer relevance of *AURKA* overexpression and loss of *CHK2* as key mediators of increased microtubule assembly rates, we determined their expression in tumour tissues from CRC ($n=333$ patients). We found a 40% frequency of *AURKA* overexpression and a 47% frequency for the loss of *CHK2* (Fig. 5a), which represents one of the most frequent genetic alterations in human CRC (ref. 31). From 325 tumour samples that could be used to simultaneously detect *AURKA* and *CHK2* expression, we calculated a proportion of 73% of the cases that exhibited at least one of the two lesions (Fig. 5b). Moreover, individual tumour specimens exhibiting loss of *CHK2* were found to be preferentially devoid of concomitant overexpression of *AURKA* (Fig. 5b). Similarly, in a panel of CRC cell lines, increased microtubule assembly rates and CIN correlated with either overexpression of *AURKA* or a loss of *CHK2* (Supplementary Fig. 5a), suggesting possible redundant functional outcomes of these two genetic alterations. This prompted us to investigate a cross-talk of aurora-A and CHK2. Not surprisingly, overexpression of *AURKA* resulted in increased levels of active and auto-phosphorylated aurora-A kinase[39] localized at mitotic centrosomes, which was associated with increased phosphorylation of the centrosomal aurora-A target protein TACC3 (ref. 40; Supplementary Fig. 5b,c). Intriguingly, however, loss of *CHK2* resulted in a very similar increase in the proportion of active aurora-A at mitotic centrosomes and an increase in TACC3 phosphorylation without altering the overall level of aurora-A (Fig. 5c and Supplementary Fig. 5d–g). As the tumour suppressor BRCA1 and, more specifically, the CHK2-mediated phosphorylation of BRCA1 (on Ser 988) was shown to be crucial for proper mitotic progression[20,21], we investigated whether CHK2 might act on aurora-A through BRCA1. Indeed, cells expressing a non-phosphorylatable *BRCA1* mutant[20,41] (S988A; Supplementary Fig. 6a) showed an increase in active aurora-A at mitotic centrosomes, which was accompanied by an increase in microtubule assembly rates (Fig. 5d,e). Moreover, in co-immunoprecipitation experiments, we detected an interaction of active aurora-A with BRCA1, which was strongly enhanced on loss of *CHK2* or loss of the CHK2-mediated phosphorylation site on BRCA1 whereas the interaction of aurora-A with its cofactor TPX2 was not affected (Supplementary Fig. 6b,c). These results suggest that the tumour suppressor CHK2 restrains the activity of the oncogenic aurora-A kinase during mitosis through the phosphorylation of the tumour suppressor protein BRCA1 and indicate that the increase in aurora-A activity might be a key trigger for increased microtubule plus-end assembly rates and influences CIN in CRC cells.

### Increased aurora-A kinase activity is a key trigger for increased microtubule assembly rates and influences CIN in CRC cells

To examine whether increased aurora-A activity is a general trigger for increased microtubule assembly rates in CRC cells, we partially inhibited aurora-A in *CHK2*-deficient HCT116 and SW620 cells using the small-molecule inhibitor MLN8054 (ref. 42), which was indeed sufficient to suppress microtubule assembly rates (Fig. 6a). In addition, we generated stable cell lines derived from *CHK2*-deficient HCT116 cells that expressed reduced levels of *AURKA*. This partial loss of aurora-A restored its proper centrosomal activity level (Supplementary Fig. 7a–c), normal microtubule assembly rates (Fig. 6b), normal mitotic spindle geometry (Fig. 6c), timely mitotic progression (Supplementary Fig. 7d) and suppressed hyper-stability of kinetochore–microtubules (Supplementary Fig. 7e). Consequently, the generation of lagging chromosomes was inhibited (Fig. 6d), which was associated with suppression of CIN (Fig. 6e and Supplementary Fig. 7f and Table 1). Importantly, partial repression of *AURKA* was also sufficient to restore normal microtubule assembly rates and to suppress CIN in various chromosomally unstable CRC cell lines irrespective of their genetic constitution but not affecting non-CIN cells (Fig. 6f,g and Supplementary Fig. 7g,h and Table 1).

Thus, these findings demonstrate that increased microtubule assembly rates resulting in CIN and commonly seen in chromosomally unstable CRC cells are dependent on elevated aurora-A kinase activity. Moreover, CIN in those cancer cells can be experimentally suppressed by different means including treatment with low-dose Taxol, partial loss of the microtubule polymerase ch-TOG or partial inhibition of aurora-A.

### Restoring proper microtubule assembly rates associated with a suppression of CIN accelerates tumour growth *in vitro* and *in vivo*

The identification of increased microtubule plus-end assembly rates as a factor influencing CIN in CRC cells and the ability to suppress this phenotype by various means enabled us to address the

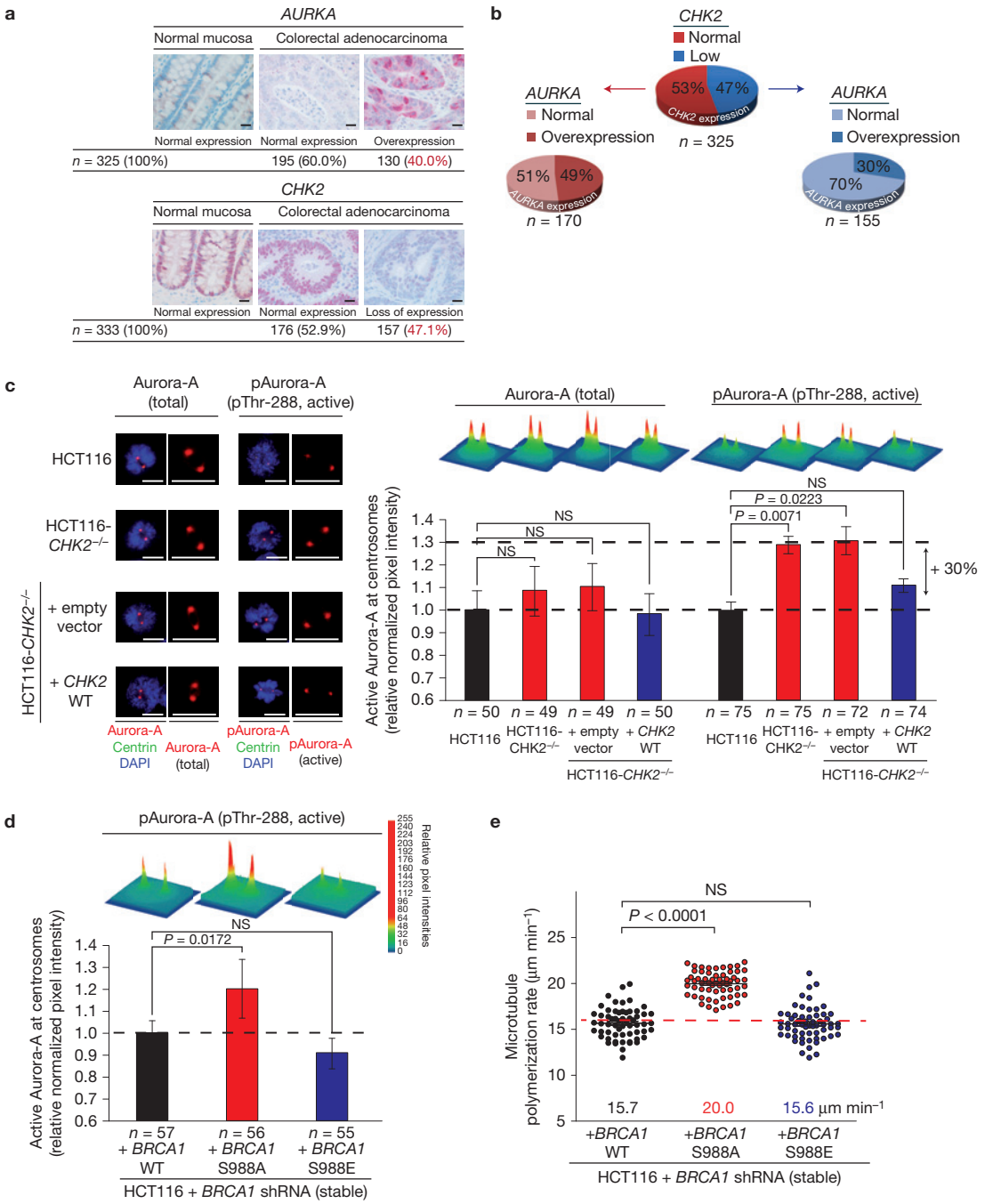


**Figure 5** The *CHK2–BRCA1* tumour suppressor pathway negatively regulates the oncogene *AURKA* to ensure proper microtubule plus-end assembly rates. (**a**) Detection of CHK2 and aurora-A proteins by immunohistochemistry analyses in tissue sections from normal mucosa and from colorectal adenocarcinomas. Examples and overall quantifications are given (scale bars, 50 μm; $n = 333$ tissue samples, *t*-test, $P = 0.001$). (**b**) Depiction of the relationship of *CHK2* and *AURKA* expression in CRC. Individual tumour samples were sub-divided on the basis of their *CHK2* expression status and subsequently analysed for their *AURKA* expression ($n = 333$ tissue samples, *t*-test, $P = 0.001$). (**c**) Detection of total and active centrosomal aurora-A (pThr-288) and centrin-2 in prometaphase cells proficient or deficient for *CHK2*. Examples of detection of aurora-A, centrin and chromosomes (DAPI) by immunofluorescence microscopy are given (scale bars, 10 μm). Signal intensities were normalized to signals for centrosomal centrin-2 and are depicted as three-dimensional surface plots and were quantified (mean ± s.e.m., *t*-test, $n = 49–50$ cells for total aurora-A and $n = 72–75$ cells for pThr-288-aurora-A from three independent experiments). NS, not significant. (**d**) Detection of increased active centrosomal aurora-A in mitotic HCT116 cells in which the endogenous BRCA1 protein was replaced by the indicated *BRCA1* mutants. Signal intensities for active aurora-A (pThr-288) at mitotic centrosomes normalized to signals obtained for centrosomal centrin-2 are depicted as three-dimensional surface plots and were quantified (mean ± s.e.m., *t*-test, $n = 55–57$ cells from three independent experiments). (**e**) Measurement of mitotic microtubule plus-end assembly rates in cells expressing either wild-type or mutant *BRCA1*. Scatter dot plots show average growth rates based on measurements of 20 microtubules per cell (mean ± s.e.m.; *t*-test, $n = 60$ cells from three independent experiments). Statistic source data for Fig. 5 can be found in Supplementary Table 2.

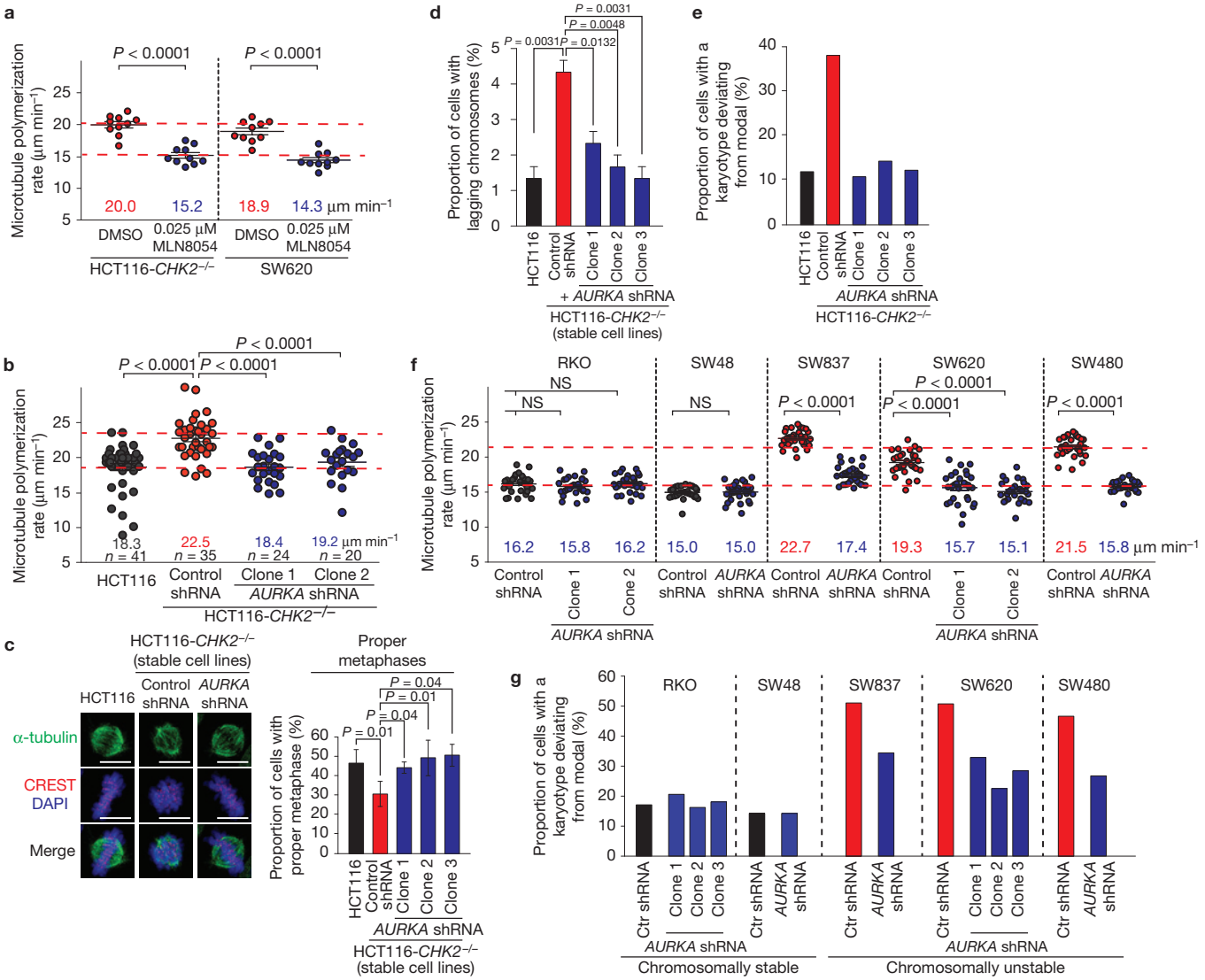


**Figure 6** Increased aurora-A kinase activity is a key trigger for increased microtubule assembly rates and CIN in CRC cells. (**a**) Measurement of mitotic microtubule plus-end assembly rates in CRC cells after partial inhibition of aurora-A by low-dose (0.025 µM) MLN8054 treatment. Scatter dot plots show average growth rates (20 microtubules per cell, mean ± s.e.m., *t*-test, $n = 10$ cells from three independent experiments). (**b**) Measurements of mitotic microtubule plus-end assembly rates in *CHK2*-deficient cells after partial repression of *AURKA*. Scatter dot plots show average microtubule assembly rates (20 microtubules per cell, mean ± s.e.m., *t*-test, $n = 20$–41 cells from three independent experiments). (**c**) Quantification of proper metaphase spindles and complete chromosome alignment in *CHK2*-deficient cells after restoration of proper microtubule assembly rates by partial repression of *AURKA*. Representative mitotic spindles are shown (scale bars, 10 µm) and proper metaphase spindles with completed chromosome alignment were quantified (mean ± s.d., *t*-test, $n = 4$–5 independent experiments with a total of 200–2,500 mitotic cells evaluated). (**d**) Detection of lagging chromosomes during anaphase in HCT116 and HCT116-*CHK2*$^{-/-}$ cells with or without partial repression of *AURKA* (mean ± s.d.; *t*-test, $n = 3$ with a total of 300 anaphase cells evaluated). (**e**) Determination of chromosome number variability in single-cell clones derived from *CHK2*-deficient cells with partial repression of *AURKA*. The proportion of cells exhibiting chromosome numbers deviating from the modal were determined ($n = 91$–100 cells). (**f**) Measurement of mitotic microtubule plus-end assembly rates in various chromosomally unstable CRC cell lines stably expressing control or *AURKA* shRNAs. Average microtubule assembly rates were determined (20 microtubules per cell, mean ± s.e.m., *t*-test, $n = 30$ cells from three independent experiments). NS, not significant. (**g**) Chromosome number variability in single-cell clones derived from various CRC cell lines and stably expressing control (ctr) or *AURKA* shRNAs. The proportion of cells exhibiting chromosome numbers deviating from the modal were determined (81–104 cells analysed per condition). Detailed data on karyotype analyses can be found in Supplementary Table 1. Statistic source data for Fig. 6 can be found in Supplementary Table 2.

long-standing question of the impact of CIN on tumour growth. As a first step in this direction, we evaluated colony formation in soft agar, which reflects anchorage-independent cell growth in tumours. Unexpectedly, *CHK2*-deficient HCT116 and SW620 cells, in which increased microtubule assembly rates and CIN were suppressed either by treatment with low-dose Taxol, by partial

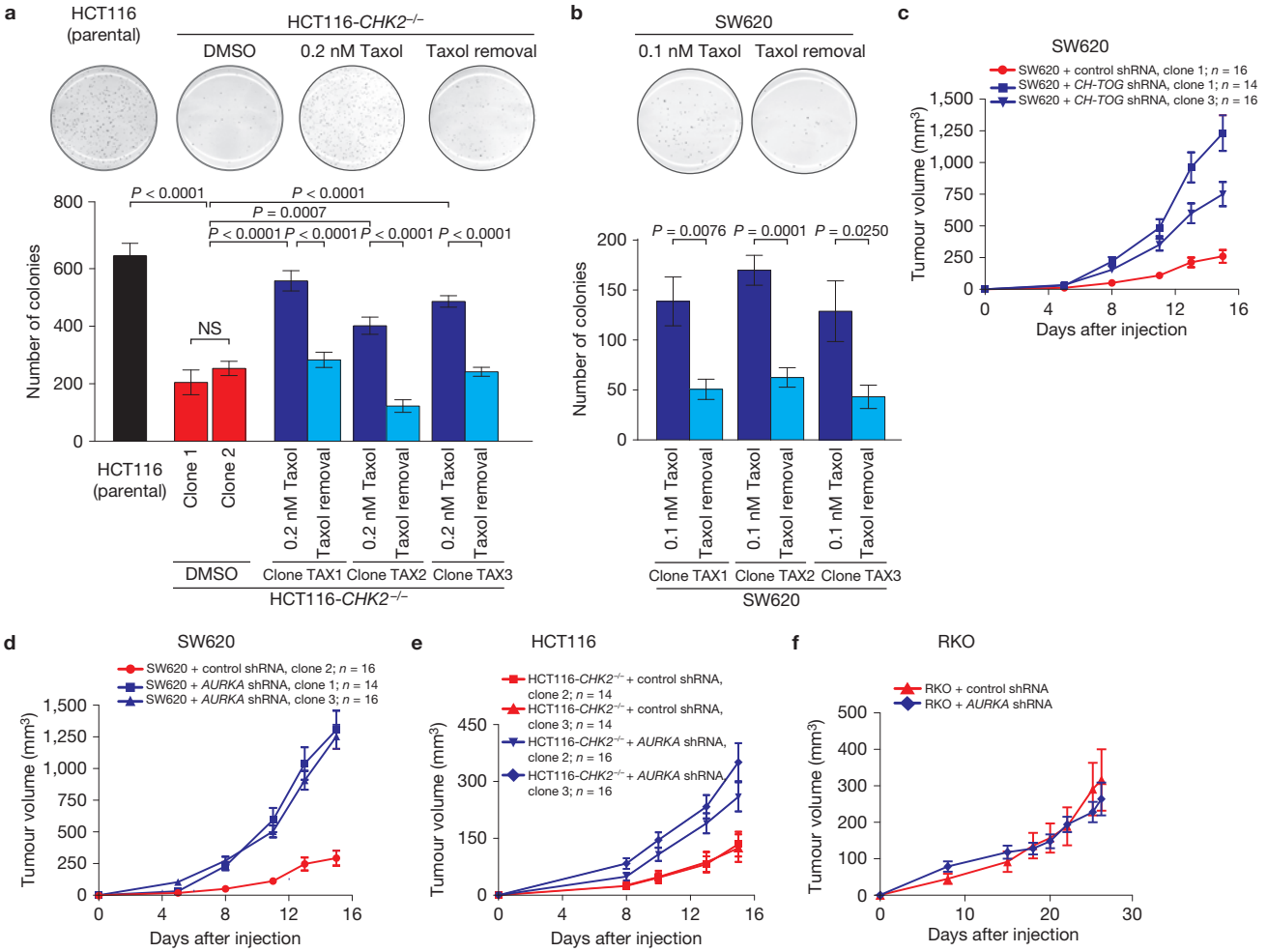


**Figure 7** Suppression of CIN by restoring proper microtubule assembly rates accelerates tumour growth *in vitro* and *in vivo*. (**a**) Determination of colony formation in soft agar of HCT116 and HCT116-*CHK2*$^{-/-}$ cells in the presence or absence of low-dose Taxol. Single-cell clones were generated and 5,000 cells were seeded onto soft agar. Three independent single cell clones grown in the presence of Taxol (TAX1, 2 and 3) were analysed. Colony numbers were quantified and the graphs show mean values ± s.e.m., *t*-test ($n = 6$ independent experiments; for HCT116: $n = 4$ independent experiments). NS, not significant. (**b**) Determination of colony formation in soft agar of SW620 cells in the presence or absence of low-dose Taxol. Single-cell clones were generated and 2,000 cells were seeded onto soft agar. Colony numbers were quantified and the graphs show mean values ± s.e.m., *t*-test ($n = 6$ independent experiments). (**c**) Xenograft tumour growth in mice after subcutaneous (s.c.) injection of chromosomally unstable SW620 expressing control or *CH-TOG* shRNAs into both flanks of nude mice. Tumour growth was monitored and tumour volumes are shown as mean values ± s.e.m. ($n = 14$–16 tumours for each group as indicated). (**d**) Xenograft tumour growth in mice after s.c. injection of chromosomally unstable SW620 expressing control or *AURKA* shRNAs into both flanks of nude mice. Tumour growth was monitored and tumour volumes are shown as mean values ± s.e.m. ($n = 14$–16 tumours for each group as indicated). (**e**) Xenograft tumour growth in mice after s.c. injection of HCT116-*CHK2*$^{-/-}$ expressing control shRNAs (chromosomally unstable) or *CHK2*-deficient cells stably expressing *AURKA* shRNAs (exhibiting restored normal microtubule assembly rates and suppressed CIN). Tumour volumes were measured over time and are shown as mean values ± s.e.m. ($n = 14$–16 tumours for each group as indicated). (**f**) Xenograft tumour growth in mice after s.c. injection of chromosomally stable RKO cells expressing control or *AURKA* shRNAs into both flanks of nude mice. Xenograft tumour growth was monitored and tumour volumes are shown as mean values ± s.e.m. ($n = 10$ tumours for each group as indicated). Statistic source data for Fig. 7 can be found in Supplementary Table 2.

repression of *CH-TOG* or by partial loss of *AURKA*, showed a significantly higher rate of colony formation in soft agar when compared with the respective cells with high CIN (Fig. 7a,b and Supplementary Fig. 8a–c). Then, we investigated the consequence of CIN triggered by an increase in microtubule assembly rates on tumour growth *in vivo*. We found that xenograft tumours derived from SW620 cells with restored microtubule assembly rates and suppressed CIN, mediated either by partial repression of *CH-TOG* or *AURKA*, exhibited significant acceleration of tumour growth *in vivo* when compared with tumours showing increased microtubule assembly rates triggering CIN (Fig. 4c,d and Supplementary Fig. 8d,e). Analyses of cells re-isolated from these xenograft tumours showed the maintenance of CIN suppression (Supplementary Fig. 8g–i). Moreover, direct comparison of xenograft tumours derived from isogenic HCT116 cells revealed that loss of *CHK2*, which is associated with increased microtubule assembly rates and CIN, caused reduced tumour growth when compared with tumour formation from parental cells (Supplementary Fig. 8f). However, restoration

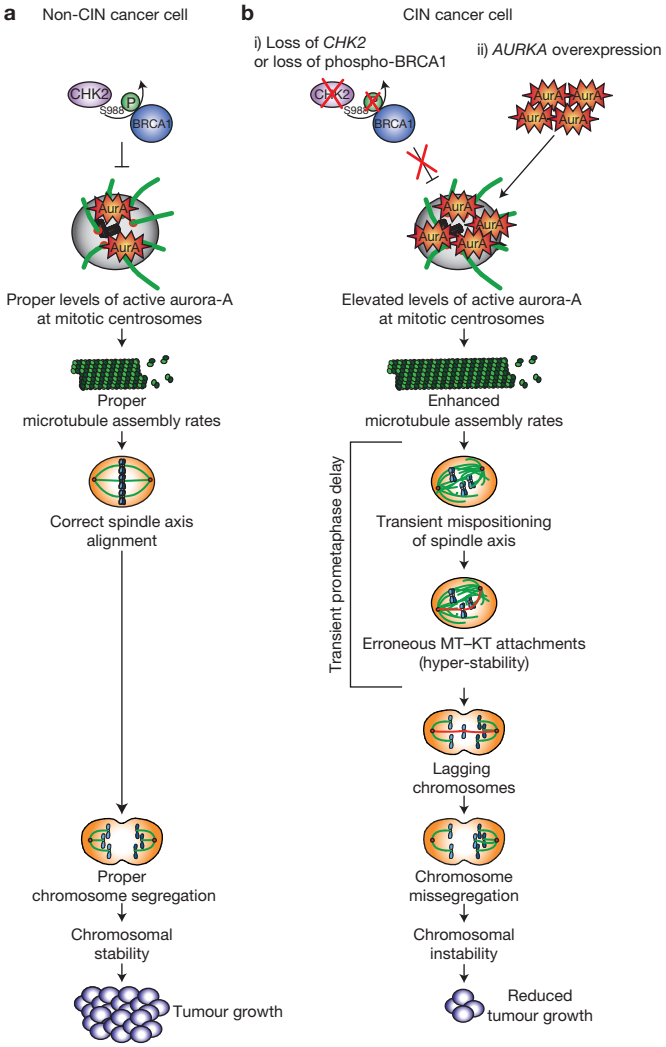


**Figure 8** Model summarizing the main findings of this report. (**a**) In chromosomally stable cancer cells, the *CHK2–BRCA1* tumour suppressor pathway is required to ensure proper levels of aurora-A activity at mitotic centrosomes. This ensures proper microtubule plus-end assembly rates as a prerequisite for proper chromosome segregation. (**b**) Either the loss of the *CHK2–BRCA1* tumour suppressor pathway or an overexpression of *AURKA* results in enhanced levels of aurora-A at mitotic centrosomes, which triggers increased microtubule assembly rates. This, in turn, causes transient spindle geometry abnormalities facilitating the generation of erroneous microtubule–kinetochore (MT–KT) attachments and lagging chromosomes as a source for chromosome missegregation. Thus, increased microtubule assembly rates influence perpetual chromosome missegregation, which is associated with reduced tumour growth *in vitro* and *in vivo*.

of normal microtubule assembly rates and chromosomal stability in those cells accelerated tumour growth to a rate very similar to that of the chromosomally stable parental HCT116 cells (Fig. 7e and Supplementary Fig. 8f). In contrast, xenograft tumours derived from chromosomally stable RKO cells with a partial loss of *AURKA* not affecting their stable karyotype did not result in acceleration of tumour growth *in vivo*, indicating that partial loss of *AURKA* does not alter the tumour growth of CRC cells *per se* (Fig. 7f). Thus, our data revealed a detrimental effect of increased microtubule assembly rates influencing CIN on tumour growth *in vitro* and *in vivo*.

## DISCUSSION

In cancer cells, CIN frequently correlates with the appearance of lagging chromosomes, which can persist either owing to impairment of error correction or owing to an increased rate of formation that might overwhelm the correction machinery[8–14,36,37]. So far, there is no evidence that error correction is frequently inactivated in human cancer cells (for example, ref. 43). However, our work now provides a mechanistic clue to the generation of lagging chromosomes as a source for CIN in CRC cells: an increase in microtubule plus-end assembly rates within mitotic spindles is frequently found in CRC cells and can trigger transient spindle geometry abnormalities that facilitate the generation of erroneous kinetochore attachments resulting in lagging chromosomes and influencing CIN (Fig. 8). This mechanism is reminiscent of a subset of cancer cells with supernumerary centrosomes[15] that show transient multipolar spindle intermediates facilitating the generation of erroneous kinetochore attachments and leading to chromosome missegregation[13,14]. It is important to note that chromosome missegregation on an increased rate of erroneous kinetochore attachments can occur in the absence of centrosome amplification and in the presence of functional error correction. It is, nevertheless, associated with a decrease in kinetochore–microtubule turnover, raising the possibility that hyper-stability of the kinetochore attachments might be related to the erroneous state of the attachment *per se*. In fact, increasing the number of erroneous attachments on monastrol washout decreases kinetochore–microtubule turnover, whereas decreasing mal attachments on prolonging error correction increases the turnover of kinetochore–microtubules. It is not yet clear whether erroneous kinetochore attachments, possibly mediated by abnormal tension within the kinetochore[7], are intrinsically more stable, but it would explain why conditions that induce erroneous kinetochore attachments without having an obvious function in error correction (for example, APC) are also associated with an increase the stability of microtubule–kinetochore attachments[37].

Our finding of an increase in microtubule assembly rates as a mechanism influencing CIN is highly cancer-relevant. Genetic alterations triggering this phenotype including an overexpression of *AURKA* or a loss of *CHK2* were found in about 70% of primary colorectal carcinomas and are also frequent in other types of cancer[18,20,44]. Thus, an increase in microtubule assembly rates, together with cancer-associated centrosome amplification, which can also be driven by overexpression of *AURKA* in certain cell types[45], might represent an important mechanism resulting in lagging chromosomes and CIN in human cancer cells.

It is not yet clear how elevated aurora-A activity causes an increase in microtubule plus-end assembly rates. Interestingly, increased microtubule assembly rates can be efficiently suppressed by repression of *CH-TOG* suggesting that this microtubule polymerase might be a target for aurora-A. In fact, the recruitment of ch-TOG to mitotic spindles is positively regulated by aurora-A-mediated phosphorylation of the adaptor protein TACC3 (refs 40,46–48) and we detected an increase in this TACC3 phosphorylation in cells with increased microtubule assembly rates. Moreover, increased microtubule assembly rates in CIN cells can also be suppressed by partially depleting TACC3 (our unpublished results), indicating that aurora-A might hyper-activate the TACC3–ch-TOG axis. In this regard, it is of note that not only an overexpression of *AURKA* (ref. 18),

but also of *TACC3* and *CH-TOG* has been linked to the etiology of various human cancers[49,50], supporting a possible link between a general hyper-activity of this microtubule plus-end assembly pathway and CIN in cancer cells.

Given the fact that we identified a new mechanism influencing CIN in CRC cells that can be suppressed by various means, we were in a position to investigate the consequences of increased microtubule assembly rates and CIN on tumour growth. As a first step into this important direction, we found that CIN cells with increased microtubule assembly rates exhibit reduced tumour growth *in vitro* and *in vivo* when compared with tumours derived from cells with proper microtubule assembly rates and suppressed CIN. Although surprising at first glance, these results might reflect a detrimental effect of aneuploidy on cell proliferation, which might be mediated by altered metabolic properties and proteotoxic stress as shown previously for yeast and mouse embryonic fibroblasts harbouring defined trisomies[51–53]. This raises the question of why cancer cells select for lesions such as *AURKA* overexpression or loss of *CHK2* causing increased microtubule assembly rates and CIN. One plausible hypothesis might be that CIN can provide a high adaptation capability, which may be crucial for tumour initiation and progression[2,3,54]. □

## METHODS

Methods and any associated references are available in the online version of the paper.

*Note: Supplementary Information is available in the online version of the paper*

### ACKNOWLEDGEMENTS

We thank B. Vogelstein, M. Grade, M. Eilers, S. Duensing, I. Hoffmann, J. Chung, O. Sibon and M. Brandeis for cell lines and plasmids. We thank F. Alves and J. Napp for providing nude mice, R. Kampe and B. Obst for excellent technical assistance and T. Beißbarth for the help with statistical analyses. We are grateful to H. Krebber, Z. Storchova and all members of the Bastians laboratory for critically reading the manuscript. This work was supported by the Molecular Diagnostic Program of the German Consortium for Translational Cancer Research funded by the Germany Ministry of Education and Research (W.W.), the grant GM069429 from the National Institutes of Health (L.W.) and the DFG, the KFO179 and by a Heisenberg professorship awarded by the DFG to H.B.

### AUTHOR CONTRIBUTIONS

N.E. and A. Stolz performed and analysed most experiments; A. Stenzinger and W.W. performed and analysed the immunohistochemistry assessment on human tumour samples, S.K., P.B. and A.A. performed and analysed the mouse xenograft experiments. L.W. performed and analysed some microtubule assembly and all fluorescence dissipation assays. H.B. designed and coordinated the study, analysed data and wrote the manuscript. All authors discussed the work and commented on the manuscript.

### COMPETING FINANCIAL INTERESTS

The authors declare no competing financial interests.

Published online at www.nature.com/doifinder/10.1038/ncb2994
Reprints and permissions information is available online at www.nature.com/reprints

1. Rajagopalan, H., Nowak, M. A., Vogelstein, B. & Lengauer, C. The significance of unstable chromosomes in colorectal cancer. *Nat. Rev. Cancer* **3,** 695–701 (2003).
2. McGranahan, N., Burrell, R. A., Endesfelder, D., Novelli, M. R. & Swanton, C. Cancer chromosomal instability: therapeutic and diagnostic challenges. *EMBO Rep.* **13,** 528–38 (2012).
3. Pfau, S. J. & Amon, A. Chromosomal instability and aneuploidy in cancer: from yeast to man. *EMBO Rep.* **13,** 515–27 (2012).
4. Gordon, D. J., Resio, B. & Pellman, D. Causes and consequences of aneuploidy in cancer. *Nat. Rev. Genet.* **13,** 189–203 (2012).
5. Thompson, S. L., Bakhoum, S. F. & Compton, D. A. Mechanisms of chromosomal instability. *Curr. Biol.* **20,** R285–R295 (2010).
6. Burrell, R. A. *et al.* Replication stress links structural and numerical cancer chromosomal instability. *Nature* **494,** 492–496 (2013).
7. Cimini, D. *et al.* Merotelic kinetochore orientation is a major mechanism of aneuploidy in mitotic mammalian tissue cells. *J. Cell Biol.* **153,** 517–527 (2001).
8. Gregan, J., Polakova, S., Zhang, L., Tolic-Norrelykke, I. M. & Cimini, D. Merotelic kinetochore attachment: causes and effects. *Trends Cell Biol.* **21,** 374–381 (2011).
9. Wordeman, L., Wagenbach, M. & von Dassow, G. MCAK facilitates chromosome movement by promoting kinetochore microtubule turnover. *J. Cell Biol.* **179,** 869–879 (2007).
10. Bakhoum, S. F., Thompson, S. L., Manning, A. L. & Compton, D. A. Genome stability is ensured by temporal control of kinetochore-microtubule dynamics. *Nat. Cell Biol.* **11,** 27–35 (2009).
11. Andrews, P. D. *et al.* Aurora B regulates MCAK at the mitotic centromere. *Dev. Cell* **6,** 253–268 (2004).
12. Lan, W. *et al.* Aurora B phosphorylates centromeric MCAK and regulates its localization and microtubule depolymerization activity. *Curr. Biol.* **14,** 273–286 (2004).
13. Ganem, N. J., Godinho, S. A. & Pellman, D. A mechanism linking extra centrosomes to chromosomal instability. *Nature* **460,** 278–282 (2009).
14. Silkworth, W. T., Nardi, I. K., Scholl, L. M. & Cimini, D. Multipolar spindle pole coalescence is a major source of kinetochore mis-attachment and chromosome mis-segregation in cancer cells. *PLoS ONE* **4,** e6564 (2009).
15. Ghadimi, B. M. *et al.* Centrosome amplification and instability occurs exclusively in aneuploid, but not in diploid colorectal cancer cell lines, and correlates with numerical chromosomal aberrations. *Genes Chromosom. Cancer* **27,** 183–190 (2000).
16. Orr, B. & Compton, D. A. A double-edged sword: how oncogenes and tumor suppressor genes can contribute to chromosomal instability. *Front. Oncol.* **3,** 164 (2013).
17. Lens, S. M., Voest, E. E. & Medema, R. H. Shared and separate functions of polo-like kinases and aurora kinases in cancer. *Nat. Rev. Cancer* **10,** 825–841 (2010).
18. Bischoff, J. R. *et al.* A homologue of Drosophila aurora kinase is oncogenic and amplified in human colorectal cancers. *EMBO J.* **17,** 3052–3065 (1998).
19. Weichert, W. *et al.* Polo-like kinase 1 expression is a prognostic factor in human colon cancer. *World J. Gastroenterol.* **11,** 5644–5650 (2005).
20. Stolz, A. *et al.* The CHK2–BRCA1 tumour suppressor pathway ensures chromosomal stability in human somatic cells. *Nat. Cell Biol.* **12,** 492–499 (2010).
21. Joukov, V. *et al.* The BRCA1/BARD1 heterodimer modulates ran-dependent mitotic spindle assembly. *Cell* **127,** 539–552 (2006).
22. Stepanova, T. *et al.* Visualization of microtubule growth in cultured neurons via the use of EB3-GFP (end-binding protein 3-green fluorescent protein). *J. Neurosci.* **23,** 2655–2664 (2003).
23. Muller, C. *et al.* Inhibitors of kinesin Eg5: antiproliferative activity of monastrol analogues against human glioblastoma cells. *Cancer Chemother. Pharmacol.* **59,** 157–164 (2007).
24. Mayer, T. U. *et al.* Small molecule inhibitor of mitotic spindle bipolarity identified in a phenotype-based screen. *Science* **286,** 971–974 (1999).
25. Brouhard, G. J. *et al.* XMAP215 is a processive microtubule polymerase. *Cell* **132,** 79–88 (2008).
26. Gard, D. L. & Kirschner, M. W. A microtubule-associated protein from Xenopus eggs that specifically promotes assembly at the plus-end. *J. Cell Biol.* **105,** 2203–2215 (1987).
27. Jordan, M. A. & Wilson, L. Microtubules as a target for anticancer drugs. *Nat. Rev. Cancer* **4,** 253–265 (2004).
28. Sironi, L. *et al.* Automatic quantification of microtubule dynamics enables RNAi-screening of new mitotic spindle regulators. *Cytoskeleton* **68,** 266–278 (2011).
29. Derry, W. B., Wilson, L. & Jordan, M. A. Low potency of taxol at microtubule minus ends: implications for its antimitotic and therapeutic mechanism. *Cancer Res.* **58,** 1177–1184 (1998).
30. Jordan, M. A., Thrower, D. & Wilson, L. Effects of vinblastine, podophyllotoxin and nocodazole on mitotic spindles. Implications for the role of microtubule dynamics in mitosis. *J. Cell Sci.* **102,** 401–416 (1992).
31. Markowitz, S. D. & Bertagnolli, M. M. Molecular origins of cancer: molecular basis of colorectal cancer. *N. Engl. J. Med.* **361,** 2449–2460 (2009).
32. Kaplan, K. B. *et al.* A role for the Adenomatous Polyposis Coli protein in chromosome segregation. *Nat. Cell Biol.* **3,** 429–432 (2001).
33. Vogel, C., Kienitz, A., Hofmann, I., Muller, R. & Bastians, H. Crosstalk of the mitotic spindle assembly checkpoint with p53 to prevent polyploidy. *Oncogene* **23,** 6845–6853 (2004).
34. Stolz, A., Ertych, N. & Bastians, H. Tumor suppressor CHK2: regulator of DNA damage response and mediator of chromosomal stability. *Clin. Cancer Res.* **17,** 401–405 (2011).
35. Luo, J. *et al.* A genome-wide RNAi screen identifies multiple synthetic lethal interactions with the Ras oncogene. *Cell* **137,** 835–848 (2009).
36. Cimini, D., Wan, X., Hirel, C. B. & Salmon, E. D. Aurora kinase promotes turnover of kinetochore microtubules to reduce chromosome segregation errors. *Curr. Biol.* **16,** 1711–1718 (2006).
37. Bakhoum, S. F., Genovese, G. & Compton, D. A. Deviant kinetochore microtubule dynamics underlie chromosomal instability. *Curr. Biol.* **19,** 1937–1942 (2009).
38. Cimini, D., Moree, B., Canman, J. C. & Salmon, E. D. Merotelic kinetochore orientation occurs frequently during early mitosis in mammalian tissue cells and error correction is achieved by two different mechanisms. *J. Cell Sci.* **116,** 4213–4225 (2003).

39. Littlepage, L. E. *et al.* Identification of phosphorylated residues that affect the activity of the mitotic kinase Aurora-A. *Proc. Natl Acad. Sci. USA* **99,** 15440–15445 (2002).
40. Kinoshita, K. *et al.* Aurora A phosphorylation of TACC3/maskin is required for centrosome-dependent microtubule assembly in mitosis. *J. Cell Biol.* **170,** 1047–1055 (2005).
41. Lee, J. S., Collins, K. M., Brown, A. L., Lee, C. H. & Chung, J. H. hCds1-mediated phosphorylation of BRCA1 regulates the DNA damage response. *Nature* **404,** 201–204 (2000).
42. Manfredi, M. G. *et al.* Antitumor activity of MLN8054, an orally active small-molecule inhibitor of Aurora A kinase. *Proc. Natl Acad. Sci. USA* **104,** 4106–4111 (2007).
43. Wood, L. D. *et al.* The genomic landscapes of human breast and colorectal cancers. *Science* **318,** 1108–1113 (2007).
44. Zhou, H. *et al.* Tumor amplified kinase STK15/BTAK induces centrosome amplification, aneuploidy and transformation. *Nat. Genet.* **20,** 189–193 (1998).
45. Wang, X. *et al.* Overexpression of aurora kinase A in mouse mammary epithelium induces genetic instability preceding mammary tumor formation. *Oncogene* **25,** 7148–7158 (2006).
46. Gergely, F., Draviam, V. M. & Raff, J. W. The ch-TOG/XMAP215 protein is essential for spindle pole organization in human somatic cells. *Genes Dev.* **17,** 336–341 (2003).
47. Lin, C. H., Hu, C. K. & Shih, H. M. Clathrin heavy chain mediates TACC3 targeting to mitotic spindles to ensure spindle stability. *J. Cell Biol.* **189,** 1097–1105 (2010).
48. LeRoy, P. J. *et al.* Localization of human TACC3 to mitotic spindles is mediated by phosphorylation on Ser558 by Aurora A: a novel pharmacodynamic method for measuring Aurora A activity. *Cancer Res.* **67,** 5362–5370 (2007).
49. Charrasse, S. *et al.* Characterization of the cDNA and pattern of expression of a new gene over-expressed in human hepatomas and colonic tumors. *Eur. J. Biochem.* **234,** 406–413 (1995).
50. Thakur, H. C. *et al.* Role of centrosomal adaptor proteins of the TACC family in the regulation of microtubule dynamics during mitotic cell division. *Biol. Chem.* **394,** 1411–1423 (2013).
51. Torres, E. M. *et al.* Effects of aneuploidy on cellular physiology and cell division in haploid yeast. *Science* **317,** 916–924 (2007).
52. Williams, B. R. *et al.* Aneuploidy affects proliferation and spontaneous immortalization in mammalian cells. *Science* **322,** 703–709 (2008).
53. Sheltzer, J. M. & Amon, A. The aneuploidy paradox: costs and benefits of an incorrect karyotype. *Trends Genet.* **27,** 446–453 (2011).
54. Duijf, P. H. & Benezra, R. The cancer biology of whole-chromosome instability. *Oncogene* **32,** 4727–4736 (2013).

DOI: 10.1038/ncb2994

## METHODS

**Human cell lines.** HCT116 and isogenic *CHK2*-deficient cells[55] were a gift from B. Vogelstein (John Hopkins University, Baltimore, Maryland, USA). Colorectal cancer cell lines were from ATCC. SW48 and derivative cell lines carrying *KRAS* mutations were from HORIZON and were generated by HORIZON's proprietary adeno-associated virus (AAV) gene targeting technology GENESIS. All cell lines were cultured at 37 °C with 5% $CO_2$ in RPMI1640 or DMEM medium containing 10% fetal calf serum, 1% glutamine, 100 μg ml$^{-1}$ streptomycin and 100 U ml$^{-1}$ penicillin (Invitrogen). All cell lines were tested for mycoplasma contamination.

**cDNAs.** HA-tagged *BRCA1* cDNAs (wild type, S988A, S988E) cloned into pcDNA3 were provided by J. Chung (NIH, Bethesda, Maryland, USA)[41]. Full-length human *AURKA* cDNA cloned into pcDNA3 (Invitrogen) was a gift from M. Eilers (Würzburg). Reconstitution of *CHK2* expression was carried out using pCEF–*CHK2* and pcDNA3–*CHK2* vectors as described previously[20]. HA-tagged human *PLK1* cloned into pcDNA3 and pCMVflag–Plk4 were gifts from I. Hoffmann (DKFZ, Heidelberg, Germany). For live-cell microscopy, pEGFP–EB3 (ref. 22) was used to detect microtubule plus-end tips. Plasmids for expression of GFP-tagged centrin and RFP-tagged H2B were gifts from S. Duensing (University of Heidelberg, Germany) and O. Sibon (University of Groningen, The Netherlands), respectively. Full-length human *MCAK* was cloned into pcDNA3 (Invitrogen).

**shRNAs and siRNAs.** The following short hairpin sequences were cloned into the pSuper-Retro vector carrying a puromycin resistance marker and were used to generate stable cell lines: *CHK2* no. 1: 5′-GCCUUAAGACACCCGU GGC-3′; *CHK2* no. 2: 5′-GAACCUGAGGACCAAGAAC-3′; *AURKA*: 5′-GGC AACCAGUGUACCUCAU-3′; *CH-TOG*: 5′-GAGCCCAGAGUGGUCCAAA-3′.

shRNA sequences targeting *BRCA1* and the shRNA resistant mutants of *BRCA1* and of *CHK2* were previously described[20]. The control scrambled shRNA sequence with no target in the human genome was: 5′-CAUAAGCUGAGAUACUUCA-3′. For transient siRNA transfections, the following siRNA sequences were used: *CHK2*: 5′-CCUUCAGGAUGGAUUUGCCAAUC-3′; *CH-TOG*: 5′-GAG CCCAGAGUGGUCCAAA-3′; *TACC3*: 5′-GUGGAUUACCUGGAGCAGU-3′; *APC*: 5′-AAGACGUUGCGAGAAGUUGGA-3′; *TP53*: 5′ -GUAAUCUACUGGGA CGGAA-3′; *MCAK*: 5′-GCAGGCUAGCAGACAAAU-3′; *LUCIFERASE*: 5′-CUU ACGCUGAGUACUUCGAUU-3′.

**Transfections and generation of stable cell lines.** Transient DNA transfections were carried out by using PEI (Sigma) or by electroporation using a BioRad electroporator (BioRad) at 300 V and 500 μF (HCT116, SW48, SW620, SW837, LS1034), 220 V and 950 μF (HT29), and 200V and 950 μF (RKO). All siRNA transfections were carried out using Interferin transfection reagent (Polyplus) according to the manufacturer's instructions. Stable transfections were carried out using Metafectene (Biontex) using the protocol from the manufacturer followed by selection in medium containing 300 μg ml$^{-1}$ G418 or 1 μg ml$^{-1}$ puromycin. Single-cell clones were isolated, expanded and further analysed. The generation of stable HCT116 cell lines with low *CHK2* expression (+ *CHK2* shRNA) and cell lines in which *CHK2* expression was reconstituted (*CHK2* knockdown plus shRNA resistant *CHK2* or *CHK2*$^{-/-}$ cells plus *CHK2* wild type) and cell lines with reduced *BRCA1* expression (HCT116 + *BRCA1* shRNA) were described in detail previously[20]. Stable colorectal cancer cell lines expressing shRNAs targeting *CH-TOG* or *AURKA* were generated by stable transfection of cells with pSuper–Retro–*CH-TOG* and with pSuper–Retro–*AURKA*, respectively and single-cell clones were subsequently selected in medium containing 1 μg ml$^{-1}$ puromycin. HCT116 cell lines stably expressing pcDNA–*AURKA* were selected in medium containing 300 μg ml$^{-1}$ G418.

**Cell treatments and cell cycle synchronization.** To synchronize cells in G2 or in mitosis, cells were first synchronized at G1/S by a double thymidine block and released into fresh medium. Six hours after the release, cells were in G2 as verified by FACS analyses and 8–9 h after release cells enter mitosis and various phases of mitosis could be observed. To block progression of mitosis beyond metaphase, 6 h after release from the thymidine block, cells were treated with 25 μM MG132 for an additional 2.5 h. To inhibit aurora-A activity, cells were treated with MLN8054 (ref. 42) at concentrations up to 0.5 μM. To restore proper microtubule plus-end growth rates low MLN8054 concentrations of 0.25 μM that partially inhibit aurora-A were used.

**Immunofluorescence microscopy.** To visualize mitotic spindles, kinetochores and centrosomes cells were fixed with 2% p-formaldehyde in PHEM (60 mM PIPES, 27 mM HEPES, 10 mM EGTA, 4 mM $MgSO_4$, pH 7.0) followed by treatment with methanol at −20 °C for 5 min. For detecting centrosomal aurora-A, cells were fixed with methanol for 6 min. The following antibodies and dilutions were used for immunofluorescence microscopy experiments: anti-α-tubulin (1:700, B-5-1-2, Santa Cruz), anti-centromere (CREST, 1:1,000, Europa Bioproducts), anti-aurora-A (1:500, H130, Santa Cruz), anti-phospho-aurora-A (pT288, 1:200, Cell Signaling), anti-γ-tubulin (1:500, GTU-88, Sigma Aldrich), anti-centrin-2 (1:250, Abcam). Secondary antibodies conjugated to Alexa Fluor-488/-594 (1:1,000, Molecular Probes) were used. Microscopy of fixed cells was performed on a Leica DM6000B microscope (Leica) equipped with a CCD (charge-coupled device) camera (Orca-II-ERA, Hamamatsu) or using a DeltaVision-ELITE microscope (Applied Precision/GE Healthcare) equipped with a CoolSnap-HQ2 camera (Photometrics). Images were recorded with a *Z*-optical spacing of 0.2 μm, deconvolved and analysed using the Leica LAS-AF software (Leica) or the SoftWorx 5.0 (Applied Precision) software. Pixel quantification of centrosomal signals was carried out using the Leica LAS-AF and ImagePro software packages (Leica; MediaCybernetics) and normalized to signal intensities derived from centrosomal signals for centrin-2. Representative examples of immunofluorescence experiments that are shown in the figures were repeated at least 3 times.

**Measurement of microtubule plus-end assembly rates.** Microtubule plus-end assembly rates were determined by tracking EB3–GFP protein in living cells[22,56]. Cells were transfected with pEGFP–EB3 (provided by L. Wordeman, University of Washington, Seattle, Washington, USA), seeded onto glass-bottom dishes (Ibidi) and after 48 h cells were treated with the Eg5 (Kif11) inhibitors monastrol (67 μM, Sigma)[24] or dimethylenastron (DME; 2 μM; Calbiochem)[23] for 2 h or left untreated. This synchronization step was useful to ensure measurements of mitotic spindles in the same mitotic phase and did not affect the plus-end growth rates *per se*. Four sections with a *Z*-optical spacing of 0.4 μm were taken every 2 s using a Deltavision ELITE microscope equipped with an Olympus ×60, 1.42 NA objective and a CoolSnap-HQ2 (Photometrics) or a PCO Edge sCMOS camera (PCO) at 37 °C, 5% $CO_2$. Images were deconvolved using the SoftWorx 5.0/6.0 software (Applied Precision). Average assembly rates (micrometres per minute) were calculated based on data retrieved for 20 individual microtubules per cell and a total of 10–60 cells were analysed in 3–4 independent experiments.

**Low-dose Taxol treatment.** To identify low, sub-nanomolar concentrations of Taxol that are sufficient to reduce the increased microtubule growth rate of SW620, SW480, SW837, HCT116-*CHK2*$^{-/-}$ and HCT116-*AURKA* cells to a level comparable to HCT116 cells without the enhanced microtubule growth phenotype, increasing, sub-nanomolar concentrations (0.05–0.5 nM) of Taxol (Sigma) were used in EB3–GFP microtubule assembly assays. The ascertained doses were used to generate single-cell clones for karyotype analyses. Subsequently, these Taxol-treated cell clones were grown for an additional 30 generations in the absence of Taxol before the karyotypes were determined again.

**Low-dose nocodazole treatment.** To identify concentrations of nocodazol that increase microtubule assembly rates, HCT116 cells were treated with various sub-nanomolar concentrations (0.5–2.5 nM) of nocodazol (Sigma) before performing EB3 tracking in live cells. For karyotype analyses, single-cell clones derived from HCT116 cells were grown in 0.5 nM nocodazol for 30 generations.

**Measurements of the half-life of kinetochore microtubule turnover.** Cells were transfected with plasmids expressing PA-GFP–tubulin and EB3–RFP to enable the laser to be focused on the kinetochore fibres before photoactivation. Late prometaphase cells were photoactivated on one side of the bipolar spindle with a 405 nm laser on a microscope imaging system equipped with a CCD camera and a ×60 1.4 NA lens (Olympus) and a QLM laser module (Personal Deltavision; Applied Precision/GE Healthcare). Images were collected using adaptive frame rates for a period of 5 min post activation. Fluorescence intensity was measured and each time point was corrected for photobleaching (the decrease over time in the fluorescence of a photoactivated mark generated in Taxol-treated cells). Each time point was also adjusted for incorporation of free photoactivated tubulin dimers using a reference point on the equivalent opposite side of the mitotic spindle[20]. Fluorescence values were normalized to the first time-point after photoactivation for each cell and the average intensity at each time point was fitted to a two-phase exponential decay curve using Prism (GraphPad Software) in which the normalized fluorescence ($F$) is described by: $F = A1\exp(-k_1 t) + A2\exp(-k_2 t)$. $A1$ represents both the rapid turnover of non-kinetochore microtubules and instantaneous diffusion of photoactivated dimers and $A2$ represents the contribution of stable kinetochore fibres, $k_1$ and $k_2$ are their respective rate constants of turnover, and $t$ is the time after photoactivation. The turnover half-life for each process was calculated as $\ln 2/k$ for each phase.

**Determination of microtubule dynamicity.** Cells were transfected with a plasmid expressing EB3–RFP and treated with 67 μM monastrol (Sigma). Microtubule plus tips were automatically tracked using plusTipTracker software as described previously[57] and overall dynamicity (collective displacement of all gap-containing tracks over their collective lifetimes), the percentage of time paused (total time all

microtubules spend in gap over the total time all tracks exist) and the catastrophe frequency (1/mean($T$), where $T$ is the lifetime (in minutes) of the growth subtrack just before the catastrophe) were determined. Rescue events could not be reliably calculated owing to the interference from the high density of tips in the monoasters.

**Determination of mitotic timing.** For live-cell analyses, cells were seeded on glass-bottom dishes (Ibidi) and transfected with H2B–GFP-expressing plasmids. Cells were followed by time-lapse microscopy at 37 °C and 5% $CO_2$ using a Leica DMI6000B (Leica). Image stacks were recorded every 2 min using a Hamamatsu EM-CCD camera (Hamamatsu) with a $Z$-optical spacing of 1 μm. Images were deconvolved and further processed using the Leica LAS-AF (Leica) or the SoftWorx 5.0/6.0 (Applied Precision) software. The time from nuclear envelope breakdown (loss of the smooth appearance of the nucleus) until the beginning of anaphase (start of chromosome movement to the poles) was determined and box and whisker plots were calculated from at least 50 recorded cells using the Prism software package, version 4 (GraphPad Software).

**Determination of spatial centrosome positioning.** Cells were transfected with pcDNA–RFP–H2B (to detect chromosomes; a gift from O. Sibon, University of Groningen, The Netherlands) and pEGFP–centrin (to detect centrioles and, thus, centrosomes; a gift from S. Duensing, University of Heidelberg, Germany) and seeded on glass-bottom dishes (Ibidi). Asynchronously growing cells were followed by time-lapse microscopy at 37 °C and 5% $CO_2$ using a DeltaVision-ELITE microscope (Applied Precision/GE Healthcare). Image stacks were recorded every minute using a PCO Edge sCMOS camera (PCO) with a $Z$-optical spacing of 1 μm. Images were deconvolved and further processed using the SoftWorx 6.0 (Applied Precision) software. When the separation of the two mother centrioles was maximal (indicating maximal separation of the two centrosomes, see also: Supplementary Videos 3 and 4), the spatial positioning of the centrosomes was determined by measuring the angle between the centrosome axis and the growth surface (substratum) considering the distance between both mother centrioles and the height from the growth surface to the centrosome in $Z$-optical spacing planes following the mathematic formula $\alpha = (\sin\alpha \times 180°)/\pi$ (see also Fig. 3d). Box plots with mean values were calculated from cells in prometaphase and metaphase using the Prism software package, version 4 (GraphPad Software).

**Detection of centrosome amplification.** For quantification of centrosome amplification, asynchronously growing HCT116 parental cells, HCT116-*CHK2*$^{-/-}$ and *AURKA*-overexpressing cells, respectively, were fixed with 2% p-formaldehyde in PHEM (60 mM PIPES, 27 mM HEPES, 10 mM EGTA, 4 mM $MgSO_4$, pH 7.0) followed by treatment with methanol at −20 °C for 5 min. Subsequently, the cells were stained for γ-tubulin (1:500, GTU-88, Sigma-Aldrich) to visualize centrosomes and with Hoechst (Hoechst 33342, 1:10,000, Biomol) to identify nuclei in interphase cells. As a positive control, HCT116 cells were transiently transfected with pCMVflag–PLK4 (provided by I. Hoffmann, DKFZ, Heidelberg, Germany), and 48 h after transfection, interphase cells with more than two γ-tubulin-positive signals were evaluated.

**Determination of lagging chromosomes.** To detect lagging chromosomes in anaphase, cells were transfected with control or *CH-TOG* siRNAs and subsequently synchronized in G1/S phase by a double thymidine block. Cells were released into medium for 8–9 h to accumulate cells in anaphase. Cells were analysed by immunofluorescence microscopy detecting CREST-positive chromosomes. Only chromosomes that were clearly separated from the two pole-oriented chromosome masses were counted as 'lagging chromosomes'. For the experiments in which the time for error correction was prolonged, cells were transfected with siRNAs targeting *CHK2*, *MCAK* or luciferase. After 48 h, cells were treated with 2 μM DME or 67 μM monastrol for 3 h, released from the block and fixed after 75 min when cells were mostly in anaphase. To prolong the time for error correction, cells were released from the DME/monastrol block into medium containing 10 μM MG132. After an additional 2.5 h, MG132 was washed out and cells were fixed 50 min later when they were mostly in anaphase.

**Western blotting.** Cells were lysed in lysis buffer (50 mM Tris-HCl, pH 7.4, 150 mM NaCl, 5 mM EDTA, 5 mM EGTA, 1% (v/v) NP-40, 0.1% (w/v) SDS, 0.1% sodium desoxycholate, protease inhibitor cocktail (Roche) and phosphatase inhibitor cocktail (Roche)). Proteins were resolved on 7.5%, 10% or 12% SDS polyacrylamide gels and blotted onto nitrocellulose or PVDF membranes using semi-dry or tank-blot procedures. For western blot experiments, the following antibodies and dilutions were used: anti-CHK2 (1:800, DCS-270, Santa Cruz), anti-β-actin (1:40,000, AC-15, Sigma), anti-BRCA1 (1:500, C-20 or D-9, Santa Cruz), anti-aurora-A (1:2,000, H130, Santa Cruz), anti-phospho-aurora-A (1:2,000, pT288, Cell Signaling), anti-phospho-aurora-A, -B, -C (1:2,000, pT288, pT232, pT198, Cell Signaling), anti-Tpx2 (1:1,000; 18D5, Santa Cruz), anti-α-tubulin (1:2,000, B-5-1-2, Santa Cruz), anti-PLK1 (1:1,000, F-8, Santa Cruz), anti-p53 (1:1,000; Ab-2, Oncogene), anti-MCAK (1:250; provided by L. Wordeman, University of Washington, Seattle, Washington, USA), anti-Axin-2 (used to verify the repression of APC; 1:1,000; Cell Signaling), anti-TACC3 (1:1,000; H300, Santa Cruz), anti-phospho-TACC3 (Ser 558, 1:1,000, D8H10, Cell Signaling), anti-CH-TOG (1:1,000; H4, Santa Cruz), secondary antibodies conjugated to horseradish peroxidase (1:10,000, Jackson ImmunoResearch). Proteins were detected by enhanced chemoluminescence. Quantification of western blot bands was performed using the ImageJ software (NIH). Representative examples of western blots that are shown in the figures were repeated at least 3 times.

**Immunoprecipitation.** Cells were lysed in 50 mM Tris-HCl, pH 7.4, 150 mM NaCl, 0.25% NP-40, 10% glycerol, 1 mM dithiothreitol, protease inhibitor and phosphatase inhibitor cocktails (Roche). Lysate (2 mg) was incubated with 1.5 μg anti-BRCA1 (D-9, Santa Cruz) or anti-Tpx2 (18D5, Santa Cruz) antibodies and immunocomplexes were precipitated using protein-G Sepharose beads (GE Healthcare).

**FACS analyses and determination of the mitotic index.** Cells were fixed in 70% ethanol overnight at 4 °C and resuspended in propidium iodide (5 μg ml$^{-1}$) and RNaseA (1 μg ml$^{-1}$) in PBS. FACS analyses were performed on a BD FACSCANTO II (Becton Dickinson) and 10,000 events were counted. Data analyses were performed using the BD FACSDIVA software (Becton Dickinson). Representative examples of cell cycle profiles that are shown in the figures were repeated at least 3 times. The mitotic index was determined by staining of fixed cells with anti-MPM2 (1:1,600, Millipore) and secondary antibodies conjugated to Alexa Fluor-488 (1:2,000, Molecular Probes) as described previously[20].

**Karyotype analyses.** Single-cell clones were generated and chromosome spread analyses and chromosome counting in individual cells was performed after 30 generations as described previously[20] and the proportion of cells with chromosome numbers deviating from the modal was determined. The chromosome number variability generated in single-cell clones within a defined time span and that showed deviation by up to 5 chromosomes was taken as a measure for CIN.

**CEP-FISH analyses.** Chromosome number variability was also determined by fluorescence *in situ* hybridization (FISH) using Aquarius Satellite Enumeration probes (Cytocell). Cells were washed with PBS and incubated in 40% (v/v) RPMI-1640 at room temperature for 15 min. Cells were then fixed in Carnoy's solution (methanol–acetic acid (3:1)). FISH was performed using α-satellite probes specific for chromosomes 7 and 15 (Cytocell) according to the manufacturer's protocol. FISH images were acquired as 0.5 μm optical sections with the ×60 1.4 NA objective and chromosome signals in at least 100 nuclei were determined.

**Human tumour samples and immunohistochemistry analyses.** Tissue samples from 333 primary human colorectal adenocarcinomas were investigated by using tissue microarrays. Microarray construction and immunohistochemical analyses were carried out as described previously[58] using a monoclonal anti-CHK2 antibody (DCS-273, 1:250, Sigma) and an anti-aurora-A antibody (clone JLM28, 1:50, Novocastra Laboratories). Staining was scored by two experienced pathologists (A. Stenzinger and W.W.). CHK2 staining could be evaluated in all cases; for *AURKA* expression, 325 cases were evaluable. Cases that showed moderate or strong expression in most tumour cells were scored as positive.

**Colony formation assays in soft agar.** To analyse anchorage-independent colony formation 6-well culture dishes were coated with 1 ml culture medium containing 1% low-melt agarose (Sigma). Subsequently, 5,000 HCT116 and 2,000 SW620 cells were re-suspended in 1 ml of growth medium containing 0.4% low-melt agarose and plated on top of the solidified bottom layer. Soft agar was overlaid with medium containing Taxol when indicated. The embedded cells were incubated at 37 °C and 5% $CO_2$ until the arising colonies were stained with 0.001% crystal violet. The growth area was scanned using a Quato IntelliScan 1600 (Quatographic Technology) and colonies were counted by using the Image-Pro Analyser v7.0 Software (Media Cybernetics).

**Mice xenografts.** HCT116 cells ($2 \times 10^6$) in 150 μl PBS were injected s.c. into both flanks of 5-week-old athymic male and female nude mice (Crl:NU-Foxn1 nu, Charles River). For SW620 xenografts, $4 \times 10^6$ SW620 cells in 200 μl PBS were injected s.c. into both flanks of 6-week-old athymic male and female mice (provided by the MEZ, University of Leipzig, Germany). Growth of two tumours per mouse was monitored regularly by determining the perpendicular diameters of the tumours. All xenograft experiments were performed according to and were approved by the

DOI: 10.1038/ncb2994

national authorities. The number of tumours analysed is given in the figure legends and in the statistic source data.

**Statistical analyses.** All data are shown as mean ± standard deviation (s.d.) or standard error of the mean (s.e.m.). Where indicated Student's *t*-tests using the Prism software package, version 4 were applied. For the signal intensities at centrosomes, the 95% confidence interval was determined. Statistical analyses on *CHK2* and *AURKA* expression patterns in human colorectal cancer tissue samples were performed using SPSS 19.0. and the significance of correlations was determined by applying two-sided Fisher's exact tests. Quantification of mitotic spindles and lagging chromosomes are based on at least 3 independent experiments, in which at least 1,500 mitotic figures or 300 anaphase cells, respectively, were evaluated. All karyotype analyses are based on quantification of individual chromosome numbers from 50–109 metaphase spreads (see also Supplementary Table 1). No statistical method was used to predetermine sample size. The experiments were not randomized and the investigators were not blinded to allocation during experiments and outcome assessment. Statistic source data are available in Supplementary Table 2.

55. Jallepalli, P. V., Lengauer, C., Vogelstein, B. & Bunz, F. The Chk2 tumor suppressor is not required for p53 responses in human cancer cells. *J. Biol. Chem.* **278,** 20475–20479 (2003).
56. Piehl, M., Tulu, U. S., Wadsworth, P. & Cassimeris, L. Centrosome maturation: measurement of microtubule nucleation throughout the cell cycle by using GFP-tagged EB1. *Proc. Natl Acad. Sci. USA* **101,** 1584–1588 (2004).
57. Applegate, K. T. *et al.* plusTipTracker: Quantitative image analysis software for the measurement of microtubule dynamics. *J. Struct. Biol.* **176,** 168–184 (2011).
58. Weichert, W. *et al.* Association of patterns of class I histone deacetylase expression with patient prognosis in gastric cancer: a retrospective analysis. *Lancet Oncol.* **9,** 139–148 (2008).

nature cell biology

DOI: 10.1038/ncb2994

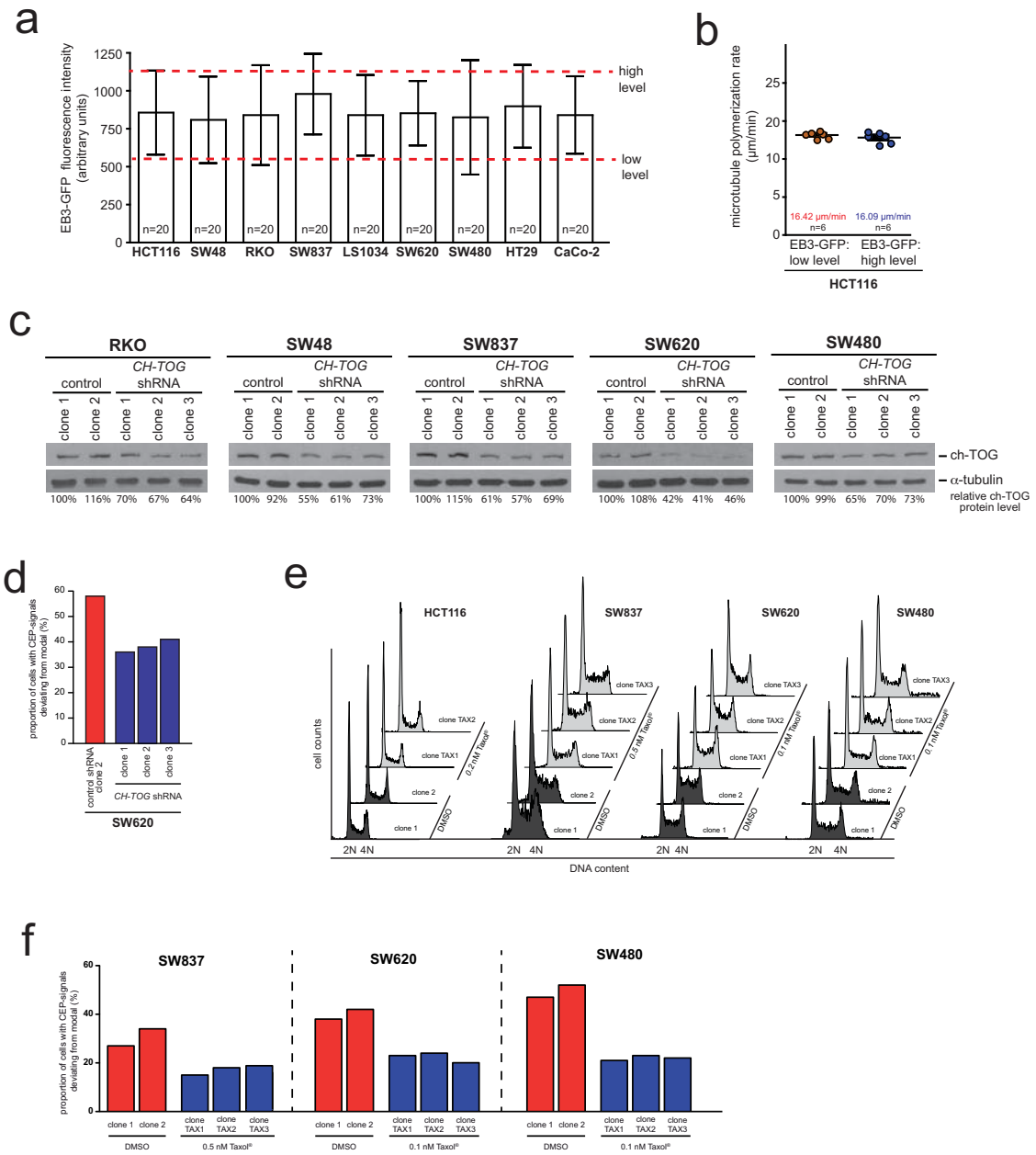


**Supplementary Figure 1** The expression level of EB3-GFP does not affect microtubule plus end assembly rates whereas partial repression of *CH-TOG/CKAP5* and low dose Taxol® treatment in various CRC cell lines suppresses chromosome number variability without affecting normal cell cycle progression. **a,** The average relative expression level of EB3-GFP is similar in all CRC cell lines investigated in microtubule assembly rate measurements. The relative expression levels of EB3-GFP were determined by quantifying the overall GFP fluorescence intensities. The graph shows mean values +/- SD (n=20 cells from 3 independent experiments). **b**, HCT116 cells with representative high or low EB3-GFP expression levels (see panel **a**) were used to measure microtubule assembly rates. Scatter dot plots show average growth rates based on measurements of 20 microtubules per cell (mean +/- SEM, *t*-test, n=6 cells from 2 independent experiments). No difference was seen in cells with low versus cells with high-level expression of EB3-GFP. **c**, Representative western blots showing protein levels for ch-TOG and α-tubulin in single cell clones derived from the indicated CRC cell lines stably expressing control or *CH-TOG/CKAP5* shRNAs. Relative ch-TOG protein levels were quantified. **d**, Karyotype analyses using CEP-FISH. Single cell clones derivative from SW620 cells expressing control or *CH-TOG/CKAP5* shRNA were grown for 30 generations and subsequently subjected to CEP-FISH analysis. The proportion of cells that deviate from the modal chromosome number of chromosome 7 and chromosome 15 was calculated (100 cells analysed per condition). **e**, FACS analyses of CRC cells after treatment with low dose Taxol® show no cell cycle impairment. Single cell clones derived from the different CRC cells lines were generated in the absence (DMSO) or presence of low dose Taxol® (0.05 - 0.5 nM). Cells were grown for 30 generations and were then subjected to FACS analyses and representative cell cycle profiles are given. **f**, Karyotype analyses using CEP-FISH. SW837, SW620 or SW480 single cell clones were grown in the presence or absence of Taxol® for 30 generations and subsequently subjected to CEP-FISH analysis. The proportion of cells that deviate from the modal chromosome number of chromosome 7 and chromosome 15 were calculated (100 cells analysed per condition). Detailed data on karyotype analyses can be found in the Supplementary Table 1. Statistic source data for Supplementary Figure 1 can be found in the Supplementary Table 2.

a

| Gene | Frequency of alteration in CRC | Association with mitosis or chromosome instability | References |
|---|---|---|---|
| *APC* | 85% (loss) | microtubule regulation chromosome alignment | Markowitz et al., 2009; Kaplan et al., 2001 |
| *TP53* | 35-55% (loss) | activated after missegregation and mitotic failure | Markowitz et al., 2009; Vogel et al., 2004 |
| *KRAS* | 35-45% (mutated) | mitotic progression synthetic lethal with *PLK1* | Markowitz et al., 2009; Luo et al., 2009 |
| *PLK1* | 60-70% (overexpressed) | centrosome function mitotic spindle assembly | Weichert et al., 2005; Lens et al., 2010 |
| *AURKA* | 20-50% (overexpressed) | centrosome function mitotic spindle assembly | Bischoff et al., 1998; Lens et al., 2010; this study |
| *CHK2* | 47% (loss) | spindle assembly chromosomal instability | Stolz et al., 2011; this study |

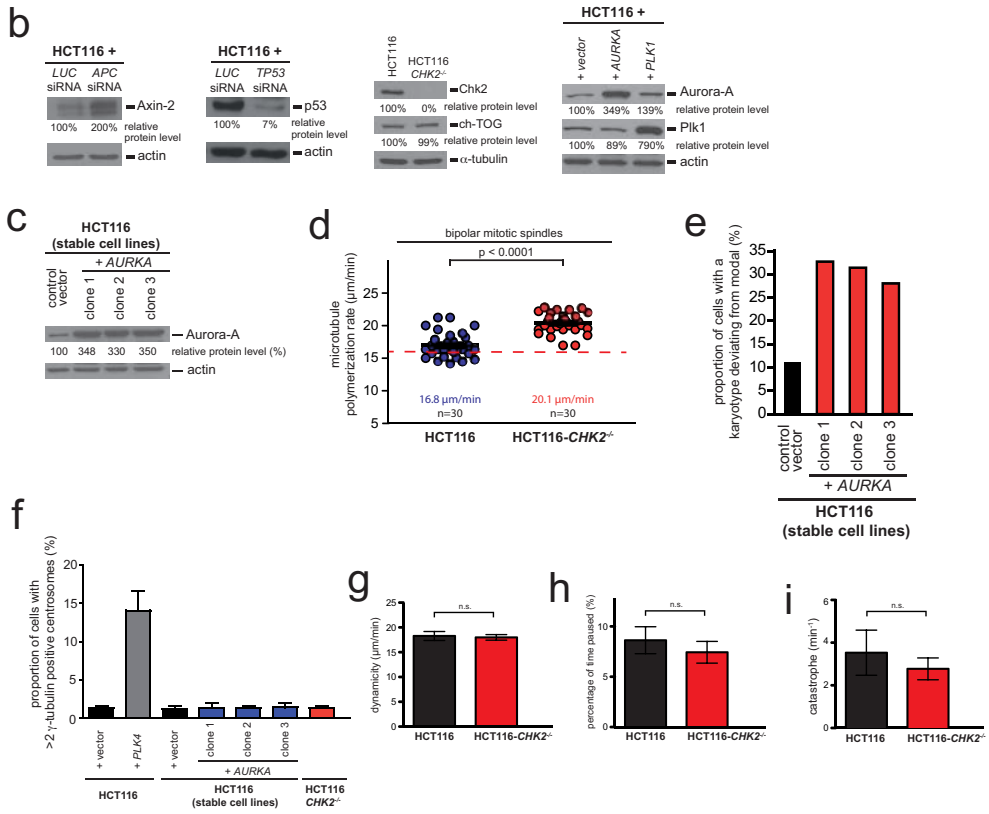


**Supplementary Figure 2** Common genetic alterations found in CRC and their impact on microtubule dynamic parameters and chromosome number variability. **a**, Genetic alterations commonly found in CRC and their implications in mitotic regulation or chromosome segregation. **b**, Representative western blots showing the loss of *APC*, *TP53* or *CHK2* or the overexpression of *AURKA* or *PLK1* in HCT116 cells after transfection with siRNAs or cDNAs or in knockout cells, respectively. Since full-length APC is hardly detectable in HCT116 cells, we detected Axin-2/conductin, which is strongly induced upon Wnt pathway activation after loss of APC. **c**, Representative western blot detecting elevated protein levels of Aurora-A in three independent cell clones derived from HCT116 cells stably overexpressing *AURKA*. **d**, Increased microtubule plus end assembly rates in bipolar mitotic spindles after loss of *CHK2*. Asynchronously growing HCT116 and isogenic *CHK2* knockout cells were subjected to microtubule assembly rate measurements in bipolar mitotic spindles. No significant difference was observed when compared to monopolar spindles measurements (see e.g. Figure 2). Scatter dot plots show average assembly rates based on measurements of 20 microtubules per cell (mean +/- SEM, *t*-test, n=30 cells from 3 independent experiments). **e**, Karyotype analyses of single cell clones derived from HCT116 cells stably overexpressing *AURKA*. Single cell clones were grown for 30 generations and the karyotype was determined (100-102 cells analysed per condition). The proportion of cells showing a deviation of the chromosome numbers from the modal within the defined time span was determined as a measure for chromosomal instability. **f**, Overexpression of *AURKA* or loss of *CHK2* does not induce supernumerary centrosomes in HCT116 cells. Three independent cell clones overexpressing *AURKA* or *CHK2* knockout cells were investigated for γ-tubulin positive interphase centrosomes. HCT116 cells transiently overexpressing *PLK4* serve as a control (mean +/- SD; n=2 with a total number of 1000 cells evaluated). **g-i**, No change in other microtubule dynamic parameters in cells with increased microtubule plus end assembly rates. The indicated cell lines expressing EB3-GFP and treated with 67 µM monastrol were live imaged at a rate of one frame per 300 ms. Microtubule tips were automatically tracked using plusTipTracker software package and **g**, dynamicity, **h**, percent of time spent paused and **i**, catastrophe frequency were determined. The graphs show mean values +/- SE, t-test (n=12 cells for each measurement). Detailed data on karyotype analyses can be found in the Supplementary Table 1. Statistic source data for Supplementary Figure 2 can be found in the Supplementary Table 2.

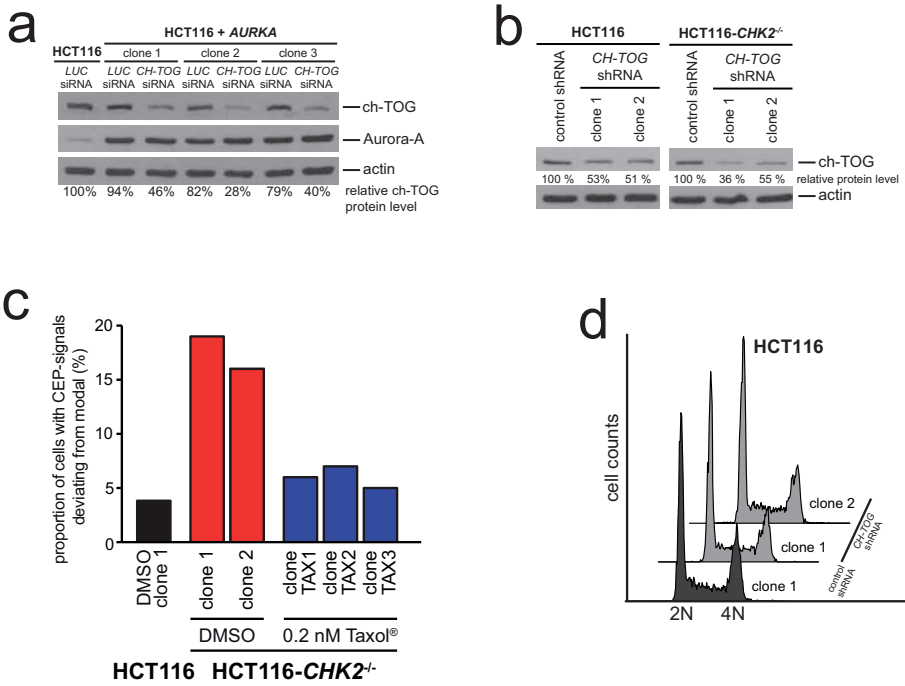


**Supplementary Figure 3** Partial repression of *CH-TOG/CKAP5* or low dose Taxol® treatment suppresses high chromosome number variability after loss of *CHK2* or *AURKA* overexpression without affecting normal cell cycle progression. **a**, Protein levels of ch-TOG and Aurora-A in HCT116 cell lines stably overexpressing *AURKA* after transient siRNA-mediated knockdown of *CH-TOG/CKAP5*. A representative western blot is shown and relative protein levels of ch-TOG were quantified. **b**, Protein levels of ch-TOG in stable *CH-TOG/CKAP5* knockdown cell lines derived from parental HCT116 or HCT116-*CHK2*$^{-/-}$ cells. A representative western blot is shown and relative protein levels were quantified. **c**, Karyotype analyses using CEP-FISH of HCT116 and HCT116-*CHK2*$^{-/-}$ single cell clones grown in the presence or in the absence of 0.2 nM Taxol® for 30 generations. The proportion of cells that deviate from the modal chromosome number of chromosome 7 and chromosome 15 were calculated (100 cells analysed per condition). **d**, Partial loss of *CH-TOG/CKAP5* does not affect normal cell cycle progression. Single cell clones were subjected to FACS analyses and representative cell cycle profiles are given. **e**, Low dose Taxol® does not affect normal cell cycle progression in cells after treatment with low dose Taxol®. Single cell clones derived from HCT116 cells overexpressing *AURKA* (clone 1) or derived from HCT116-*CHK2*$^{-/-}$ cells were generated in the presence of DMSO or 0.2 nM Taxol®. After 30 generations cells were subjected to FACS analyses and representative cell cycle profiles are given. Detailed data on karyotype analyses can be found in the Supplementary Table 1. Statistic source data for Supplementary Figure 3 can be found in the Supplementary Table 2.

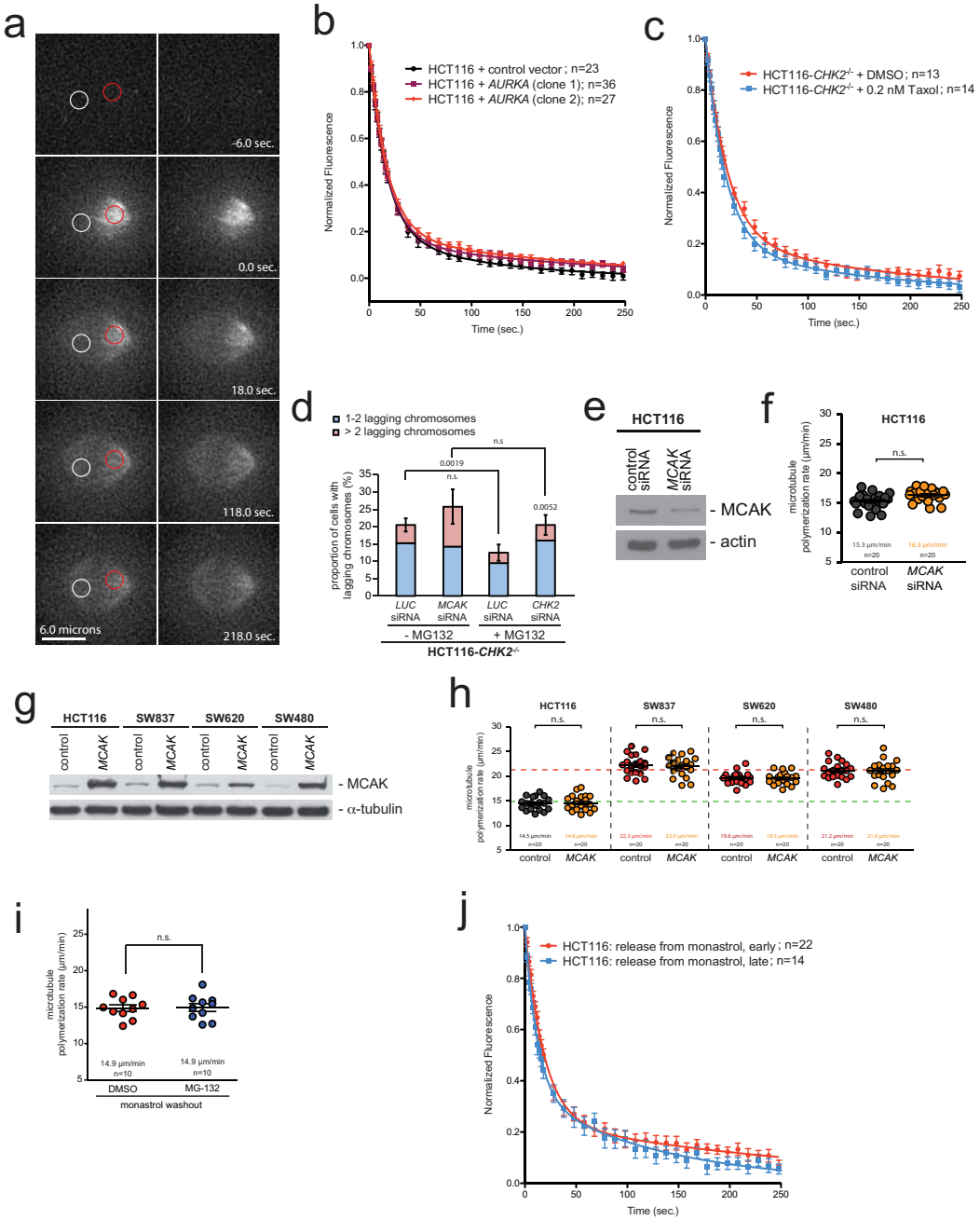


**Supplementary Figure 4** Increased microtubule assembly rates and impaired error correction are separable mechanisms. **a**, Determination of microtubule turnover. Examples of time-lapse fluorescent images of HCT116 spindles before (-6.0 s) and after photo-activation of GFP-tubulin. Scale bar, 6 μm. **b-c**, Normalized fluorescence intensity over time after photo-activating spindles of HCT116 cells with and without *AURKA* overexpression or loss of *CHK2* (mean +/- SEM, n=13-36 cells as indicated). **d**, Quantification of the proportion of lagging chromosomes in HCT116-*CHK2*$^{-/-}$ cells with and without siRNA-mediated knockdown of *MCAK* after monastrol washout and after release from monastrol into MG132 to prolong the time for error correction (mean +/- SD, *t*-test, n=4 independent experiments with a total number of 400 cells evaluated). **e**, Representative western blots showing the loss of *MCAK* in HCT116 cells after transfection with siRNAs. **f**, Repression of *MCAK* does not alter microtubule plus end assembly rates. HCT116 cells were transfected with a siRNA targeting *MCAK* and microtubule plus end assembly rates were determined. Scatter dot plots show average growth rates based on measurements of 20 microtubules per cell (mean +/- SEM, *t*-test, n=20 cells from 3 independent experiments). **g**, Representative western blots showing protein levels for MCAK in different CRC cells lines overexpressing human *MCAK*. **h**, Overexpression of *MCAK* in CIN cells does not alter microtubule plus end assembly rates. Different CRC cells overexpressing *MCAK* were used to determine microtubule plus end assembly rates. Scatter dot plots show average growth rates based on measurements of 20 microtubules per cell (mean +/- SEM, *t*-test, n=20 cells from 3 independent experiments). **i**, Determination of microtubule plus end assembly rates in HCT116 cells after monastrol washout and after release from monastrol into MG132. Scatter dot plots show average microtubule assembly rates based on measurements of 20 microtubules per cell (mean +/- SEM, *t*-test, n=10, cells from 2 independent experiments). **j**, Determination of kinetochore-microtubule turnover. Normalized fluorescence intensities over time after photoactivation of spindles in HCT116 cells expressing PA-GFP-tubulin immediately after establishing bipolar spindles upon release from monastrol (early) and after release from monastrol into MG132 (late) (mean +/- SEM, n=14-33 cells as indicated at 33 time points each). Statistic source data for Supplementary Figure 4 can be found in the Supplementary Table 2.

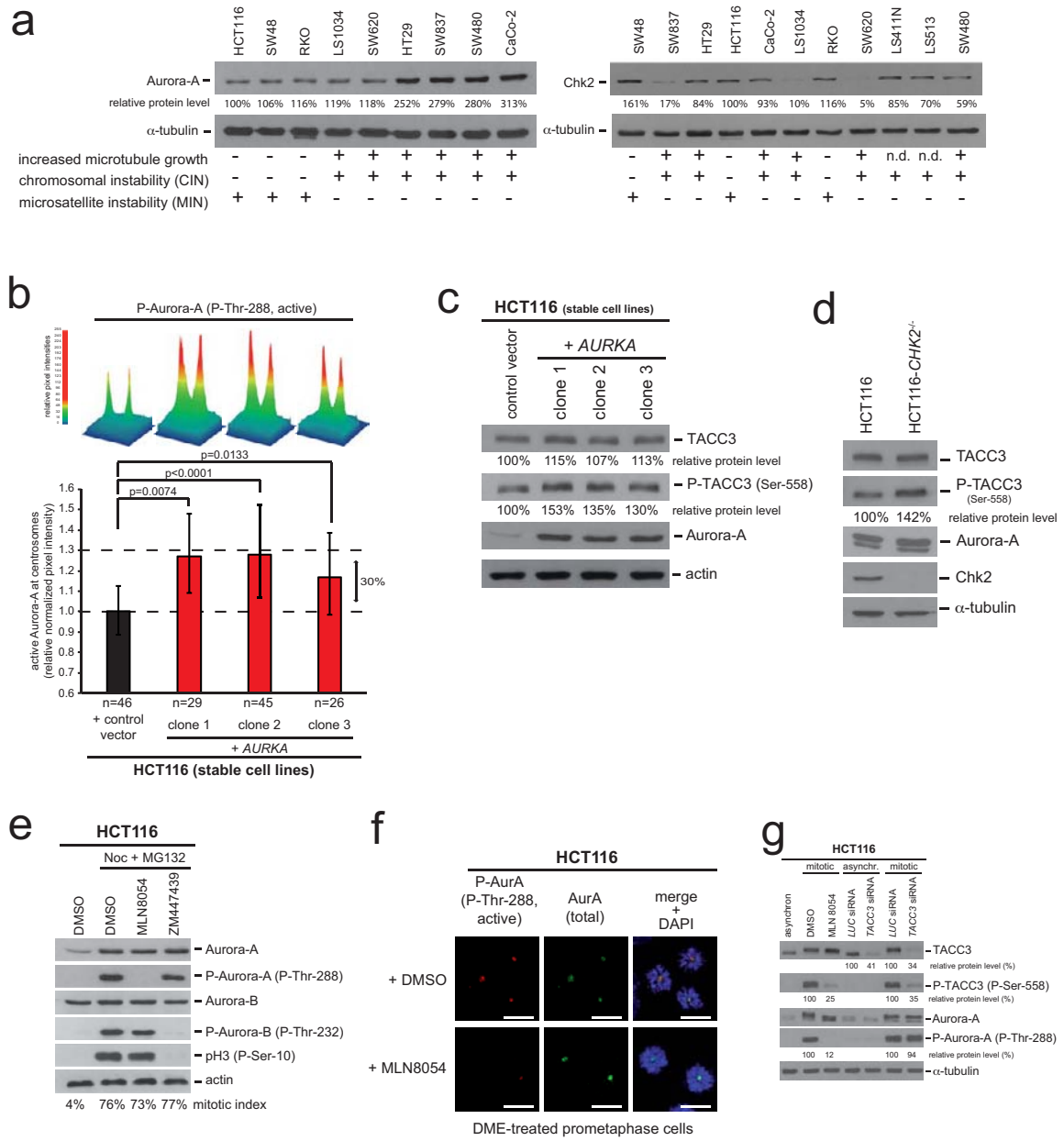


**Supplementary Figure 5** Overexpression of *AURKA* or loss of *CHK2* in CRC cell lines results in elevated levels of active centrosomal Aurora-A and increased TACC3 phosphorylation. **a**, Representative western blots showing Aurora-A (left panel) and Chk2 (right panel) protein levels in the indicated CRC cell lines. Note that chromosomally instable CRC cells exhibiting enhanced microtubule growth rates show preferentially either an overexpression of *AURKA* or a loss of *CHK2* correlating with increased microtubule growth rates and chromosomal instability. **b**, Overexpression of *AURKA* causes increased centrosomal levels of active Aurora-A (auto-phosphorylated at threonine-288). Active Aurora-A (pT288) was detected in HCT116 prometaphase cells stably overexpressing *AURKA* using phospho-specific antibodies in immunofluorescence microscopy experiments. Signal intensities for centrosomal pT288 and normalized to signals obtained for centrosomal centrin are depicted as 3D surface plots and quantified (mean, +/-95%-CI, *t*-test, 26-46 cells as indicated, 3 independent experiments). **c**, Increased phosphorylation of TACC3 upon overexpression of *AURKA* in HCT116 cells. Representative western blots showing protein levels of Aurora-A, Chk2, TACC3 and TACC3 phosphorylated at Ser-558 in HCT116 cells stably overexpressing *AURKA* and synchronized in mitosis (DME 16 hours). **d**, Increased levels of phosphorylated TACC3 in *CHK2* deficient cells. Representative western blots are shown. **e**, Determination of the specificity of the antibodies used to detect phosphorylated Aurora-A and TACC3. Representative western blots detecting total and active forms of Aurora-A in HCT116 cells synchronized in mitosis (nocodazole 14.5 hours -> MG132 1.5 hours to prevent mitotic exit) after specific inhibition of Aurora-A (0.5 μM MLN8054) or Aurora-B (2 μM ZM447439). Mitotic indices are shown. **f**, Treatment of mitotic cells with MLN8054 abolishes centrosomal signals for active Aurora-A (pT288). HCT116 cells were treated with DME for 3.5 hours and subsequently treated with DMSO or 0.5 μM MLN8054 for additional 30 min. Total and active (P-Thr-288) Centrosomal Aurora-A was detected by immunofluorescence microscopy (active Aurora-A, red; total Aurora-A, green; DNA, blue; scale bar, 10 μm). Representative examples of immunofluorescence microscopy pictures are shown. **g**, Specificity of the antibodies used to detect the Aurora-A mediated phosphorylation of TACC3. HCT116 cells were transfected with the indicated siRNAs and synchronized in mitosis by DME treatment and subsequently treated with DMSO or 0.5 μM MLN8054. TACC3 and phosphorylated TACC3 as well as total Aurora-A and active Aurora-A were detected on western blots. Representative western blots are shown. Statistic source data for Supplementary Figure 5 can be found in the Supplementary Table 2.

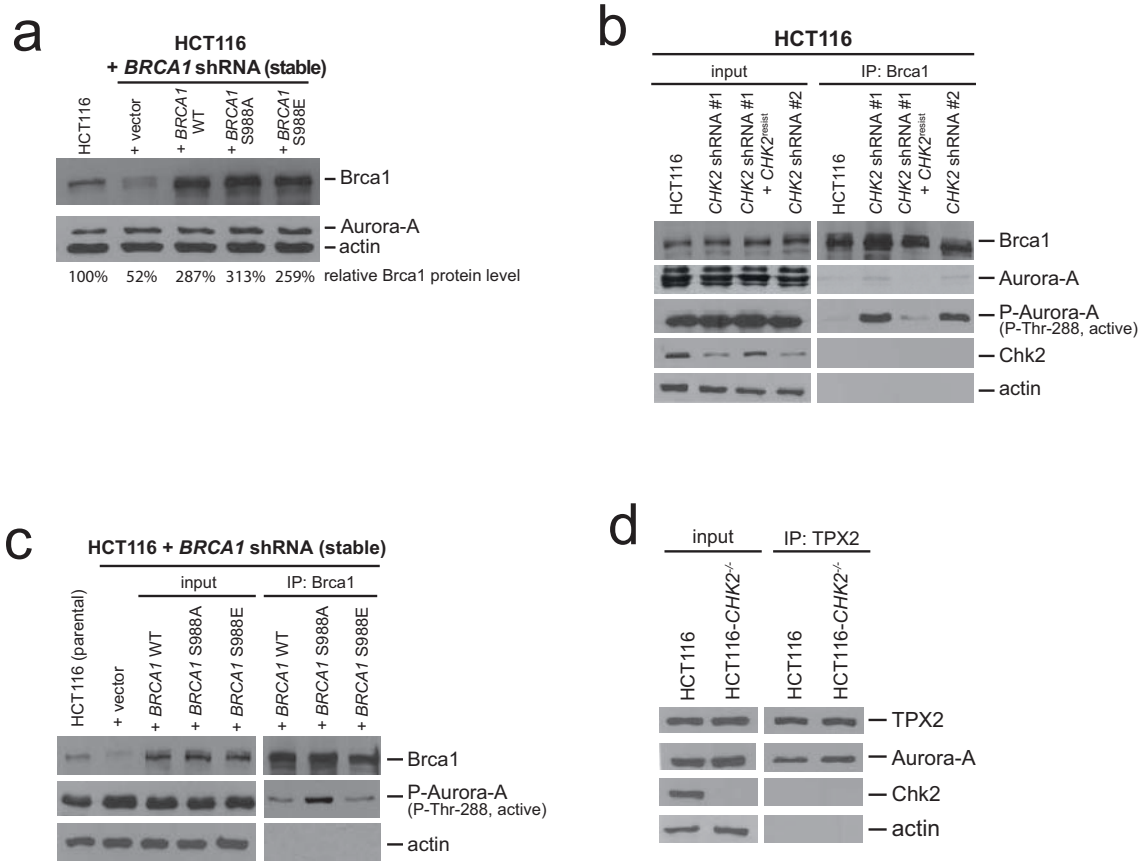


**Supplementary Figure 6** Loss of *CHK2* or loss the Chk2-mediated phosphorylation of Brca1 causes enhanced interaction of Brca1 with active Aurora-A. **a**, Representative western blots showing the re-expression of wild type (WT), non-phosphorylatable (S988A) and phospho-mimetic (S988E) mutants of Brca1 in HCT116 cells stably expressing shRNAs targeting endogenous *BRCA1*. Relative protein levels were quantified. **b**, The interaction of Brca1 with active Aurora-A is increased when Chk2 is decreased. Immunoprecipitation of Brca1 from whole cell lysates derived from HCT116 cells with or without low levels of Chk2 (mediated by stable expression of shRNAs targeting *CHK2*) or after reconstitution of *CHK2* expression (mediated by stable expression of shRNA resistant mutant of *CHK2*). Cells were synchronized in mitosis, Brca1 was immunoprecipitated and associated Aurora-A and active Aurora-A proteins (auto-phosphorylated at threonine-288; P-Aurora-A) were subsequently detected on western blots. Active Aurora-A bound to Brca1 is significantly enhanced when *CHK2* expression is repressed. Representative western blots are shown. **c**, The interaction of Brca1 with active Aurora-A is increased after loss of the Chk2 phosphorylation site of Brca1. Immunoprecipitation of Brca1 from mitotic synchronized, stable HCT116 + *BRCA1* shRNA cells expressing either a wild type (WT), a non-phosphorylatable mutant (S988A) or a phospho-mimetic mutant (S988E) of *BRCA1* and subsequent detection of active Aurora-A (P-Aurora-A, P-Thr288). Brca1, which cannot be phosphorylated by Chk2 shows an enhanced interaction with the active form of Aurora-A. Representative western blots are shown. **d**, Control immunoprecipitation experiments showing that the interaction of Aurora-A with its co-factor TPX2 is not altered in the absence of *CHK2*. Immunoprecipitation of TPX2 from *CHK2* proficient (HCT116) or deficient (HCT116-*CHK2*$^{-/-}$) mitotic synchronized cells and subsequent detection of Aurora-A on western blots. Representative western blots are shown.

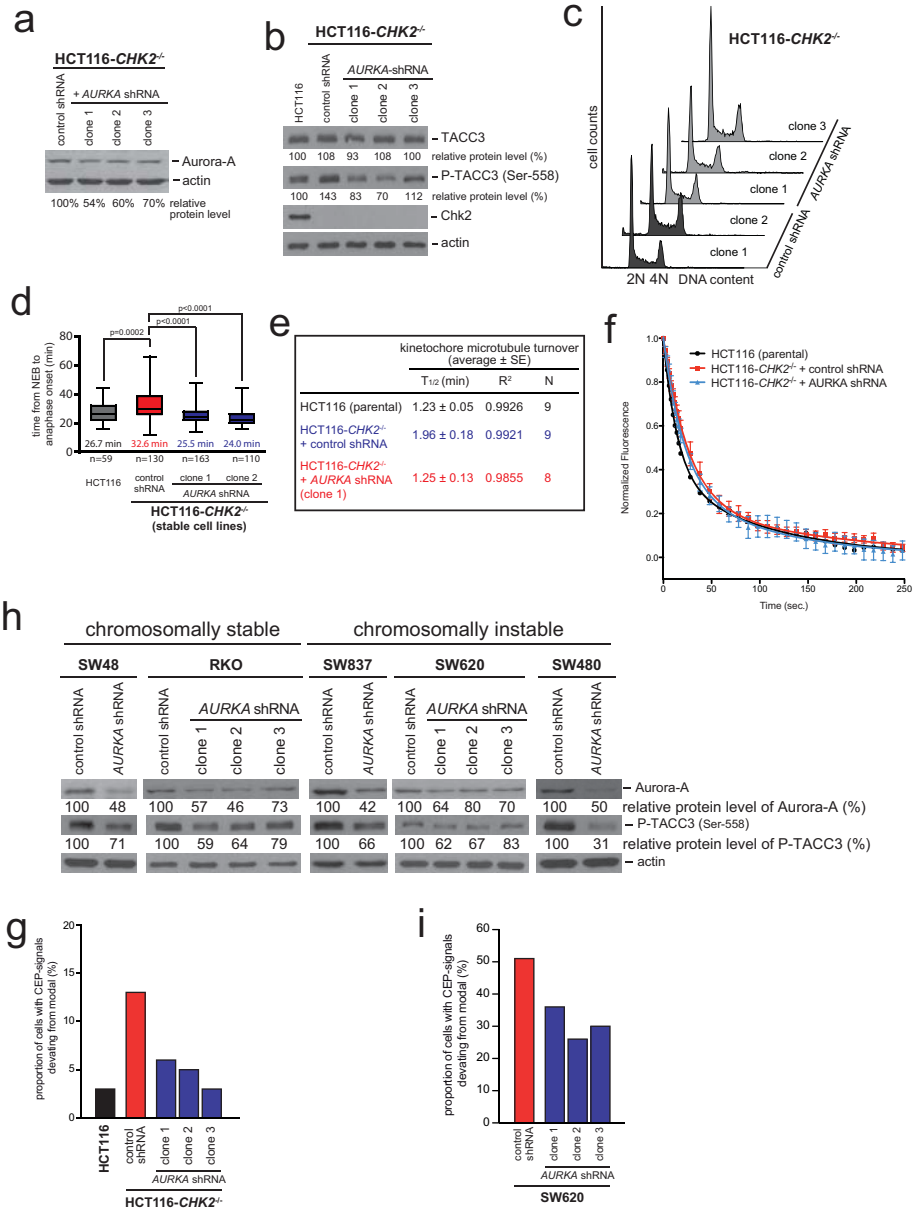


**Supplementary Figure 7** Partial loss of *AURKA* in CRC cell lines restores normal mitotic progression, kinetochore microtubule turnover and chromosomal stability without affecting normal cell cycle progression. **a**, Representative western blots showing reduced protein levels of Aurora-A in HCT116-*CHK2*$^{-/-}$ cells stably expressing *AURKA* shRNAs. **b**, Representative western blots showing reduced phosphorylation of TACC3 (P-Ser-558) in HCT116-*CHK2*$^{-/-}$ cells after partial loss of *AURKA*. **c**, Partial loss of *AURKA* in *CHK2* deficient cells does not affect cell cycle progression. Stable cell lines expressing shRNAs targeting *AURKA* were subjected to FACS analyses. Representative cell cycle profiles are shown. **d**, Partial loss of *AURKA* in HCT116-*CHK2*$^{-/-}$ cells restores normal mitotic timing. The time from nuclear envelope breakdown (NEB) to anaphase onset was determined by live cell microscopy. The box and whisker plot shows the range, median and quartile of the measurements (*t*-test, n=59-163 cells as indicated, 3 independent experiments). **e**, Partial loss of *AURKA* suppresses hyper-stable kinetochore-microtubule attachments in cells with increased microtubule assembly rates. The indicated cell lines expressing photo-activatable GFP-tubulin (PA-GFP-tubulin) were used to determine kinetochore-microtubule turnover and a summary of the measurements is given (SEM, n=8-9 cells as indicated, 3 independent experiments). **f**, Determination of kinetochore-microtubule turnover. The graph displays normalized fluorescence intensities over time after photoactivation of spindles in HCT116-*CHK2*$^{-/-}$ and cells expressing shRNAs targeting *AURKA* clone 1 (mean +/- SEM, n=8-9 cells as indicated, 3 independent experiments). **g**, Karyotype analyses of HCT116-*CHK2*$^{-/-}$ cells after partial repression of *AURKA* using CEP-FISH. Single cell clones derived from HCT116-*CHK2*$^{-/-}$ cells expressing control or *AURKA* shRNAs were grown for 30 generations and subsequently subjected to CEP-FISH analysis. The proportion of cells that deviate from the modal chromosome number of chromosome 7 and chromosome 15 were calculated (100 cells analysed per condition). **h**, Representative western blots showing the protein levels of Aurora-A and phosphorylated TACC3 (P-Ser-558) in various CRC cell lines stably expressing control or shRNAs targeting *AURKA*. **i**, Karyotype analyses of SW620 cells after partial repression of *AURKA* using CEP-FISH. Single cell clones derived from SW620 cells expressing control or *AURKA* shRNAs were grown for 30 generations and subsequently subjected to CEP-FISH analysis. The proportion of cells that deviate from the modal chromosome number of chromosome 7 and chromosome 15 were calculated ( 100 cells analysed per condition). Detailed data on karyotype analyses can be found in the Supplementary Table 1. Statistic source data for Supplementary Figure 7 can be found in the Supplementary Table 2.

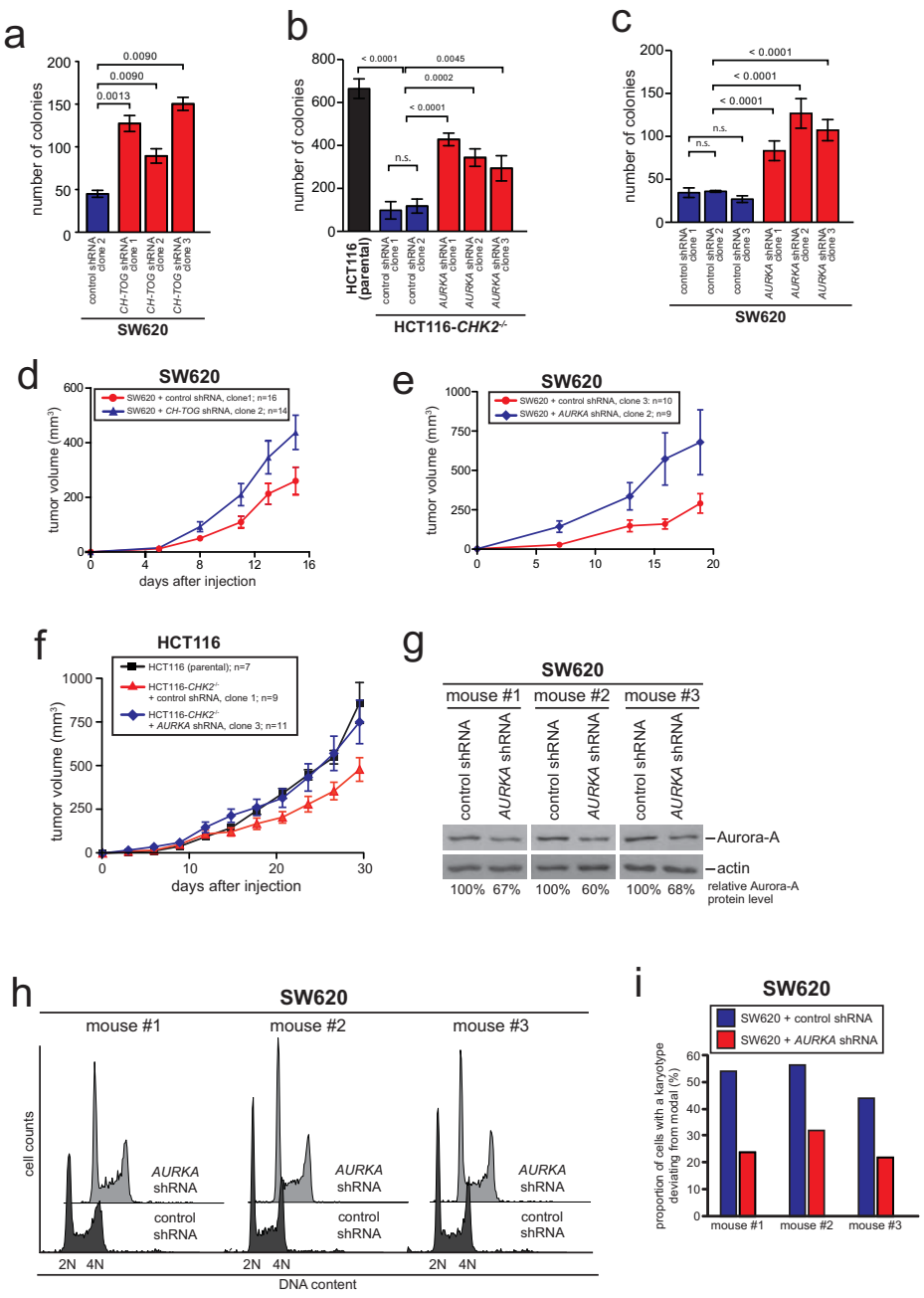


**Supplementary Figure 8** Restoration of normal microtubule assembly rates and chromosomal stability accelerates CRC tumor growth *in vitro* and *in vivo*. **a-c,** Accelerated colony formation activity of SW620 and HCT116-*CHK2*$^{-/-}$ cells after partial loss of *CH-TOG* or *AURKA*. Stable SW620 cell lines expressing control, *CH-TOG* shRNAs or *AURKA* shRNAs were subjected to colony formation assays in soft agar (2,000 cells per well) and colonies were counted. **a**: 2,000 cells per well, mean +/- SEM, *t*-test, n=3 independent experiments. **b,** 5,000 cells per well, mean +/- SEM, *t*-test, n=4-6, 4-6 independent experiments. **c**: 2,000 cells per well, mean +/- SEM, *t*-test, n=4 independent experiments. **d-f,** Growth of xenograft tumors derived from SW620 or HCT116 cells as indicated with or without partial repression of *CH-TOG/CKAP5* or *AURKA*. The indicated cells were injected s.c. into both flanks of the mice and tumor volumes were determined over time. **d**, The experiment shown is an extension to the experiment shown in Figure 7c using an independent *CH-TOG/CKAP5* shRNA expressing clone (mean +/- SEM, n=14-16 tumors as indicated). **e,** The experiment shown is an independent extension to the experiment shown in Figure 7d and additional clones were used (mean +/- SEM, n=9-10 tumors as indicated). **f**, The experiment shown is an independent extension to the experiment shown in Figure 7e and additional clones were used (mean +/- SEM, n=7-11 tumors as indicated). **g,** Xenograft tumors maintain the partial repression of *AURKA* *in vivo*. Cells were re-isolated from three different SW620 xenograft tumors grown in three different mice and expressing control (clone 1) or *AURKA* shRNAs (clone 1). Cells were subjected to western blotting and protein levels of Aurora-A were detected. Representative western blots are shown. **h**, Tumor cells re-isolated from xenograft tumors do not show gross alterations in cell cycle distribution. Cells re-isolated from the different xenograft tumors were subjected to FACS analyses and representative cell cycle profiles are shown. **i**, The suppression of CIN in SW620 cells with reduced *AURKA* expression is maintained in xenograft tumors *in vivo*. Tumor cells re-isolated from xenograft tumors were subjected to karyotype analyses (50 cells per condition). Detailed data on karyotype analyses can be found in the Supplementary Table 1. Statistic source data for Supplementary Figure 7 can be found in the Supplementary Table 2.

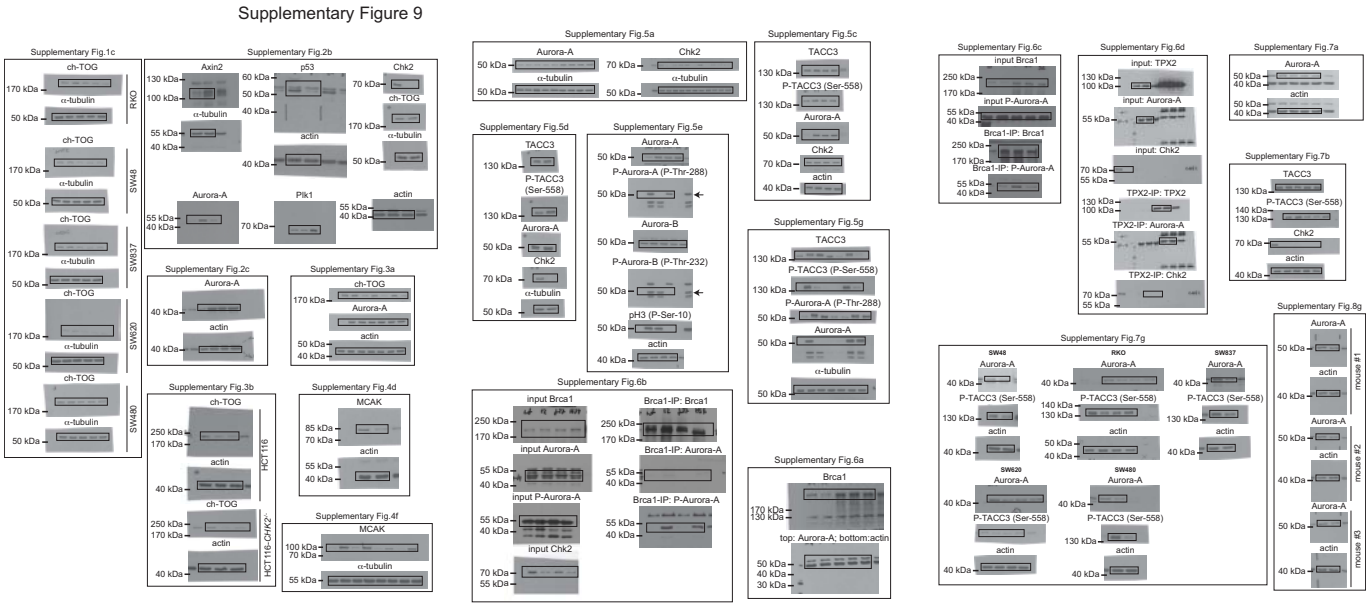


**Supplementary Figure 9** Scans of western blots.

**Supplementary Table Legends**

**Supplementary Table 1** Summary of karyotype analyses. For each experiment the numbers of individual chromosomes per metaphase spread were determined and are listed as indicated. For the CEP-FISH analyses the gains and losses of chromosomes 7 and 15 were determined and are listed for each experiment as indicated.

**Supplementary Table 2** Statistic source data.

**Supplementary Video Legends**

**Supplementary Video 1** Accurate spindle assembly and mitotic progression of HCT116 cells. Time-lapse fluorescence microscopy movie showing an example of an asynchronously growing HCT116 cell expressing GFP-tagged H2B and RFP-tagged tubulin and progressing through mitosis. The cell shows a correct spindle assembly and geometry and a timely progression through mitosis (red; mCherry-α–tubulin ; green; pEGFP-H2B). Images with 12 z-stacks were recorded every 2 minutes, deconvolved and maximal projections are shown. The movie has a speed of 5 frames per second. The scale bar represents 15 µm.

**Supplementary Video 2** Abnormal spindle assembly and delayed mitotic progression of HCT116 cells after loss of *CHK2*. Time-lapse fluorescence microscopy movie showing an example of an asynchronously growing HCT116-*CHK2*$^{-/-}$ cell expressing GFP-tagged H2B and RFP-tagged tubulin and progressing through mitosis. The cell shows transient abnormalities in spindle structure and geometry associated with lagging chromosomes appearing during anaphase (red; mCherry-α–tubulin ; green; pEGFP-H2B). Images with 12 z-stacks were recorded every 2 minutes, deconvolved and maximal projections are shown. The movie has a speed of 5 frames per second. The scale bar represents 15 µm.

**Supplementary Video 3** Accurate centrosome positioning in HCT116 cells. Time-lapse fluorescence microscopy movie showing an example of a HCT116 cell expressing RFP-tagged H2B and GFP-tagged centrin during mitosis. The cell shows the separation of the centrioles during prophase and prometaphase (red; pcDNA-RFP-ruby-H2B; green; pEGFP-Centrin). At the time point when centrosome separation was maximal this kind of movie was used to calculate the spatial positioning of the centrosomes as depicted in Figure 3d. Images with 14 z-stacks were recorded every minute, deconvolved and maximal projections are shown. The movie has a speed of 5 frames per second. The scale bar represents 15 µm.

**Supplementary Video 4** Centrosome mispositioning in HCT116 cells after loss of *CHK2*. Time-lapse fluorescence microscopy movie showing an example of a HCT116-*CHK2*$^{-/-}$ cell expressing RFP-tagged H2B and GFP-tagged centrin and progressing through mitosis. The cell shows the separation of the centrioles during prophase and prometaphase, which is not significantly altered when compared to the parental cell shown in Supplementary Video 3 (red; pcDNA-RFP-ruby-H2B; green; pEGFP-Centrin). At the time point when centrosome separation was maximal this kind of movie was used to calculate the spatial positioning of the centrosomes as depicted in Figure 3d. Images with 14 z-stacks were recorded every minute, deconvolved and maximal projections are shown. The movie has a speed of 5 frames per second. The scale bar represents 15 µm.

**Supplementary Table 1: Karyotype analyses, chromosome counting**

**related to Figure 1c**

| | | | numbers of chromosomes per metaphase | | | | | | | | | |
|---|---|---|---|---|---|---|---|---|---|---|---|---|
| **cell line:RKO (stable ch-TOG knockdown)** | **percent of cells with a karyotype deviating from modal** | **metaphases analyzed** | **44** | **45** | **46** | **47** | **48** | **49** | **50** | **51** | **52** | **53** |
| RKO + control shRNA, clone 1 | 25 | 100 | 0 | 0 | 0 | 8 | 14 | 75 | 3 | 0 | 0 | 0 |
| RKO + control shRNA, clone 2 | 27 | 103 | 0 | 0 | 0 | 3 | 9 | 15 | 75 | 1 | 0 | 0 |
| RKO + ch-TOG shRNA, clone 1 | 28 | 78 | 0 | 0 | 0 | 3 | 45 | 25 | 5 | 0 | 0 | 0 |
| RKO + ch-TOG shRNA, clone 2 | 30 | 50 | 0 | 0 | 0 | 3 | 35 | 9 | 1 | 2 | 0 | 0 |
| RKO + ch-TOG shRNA, clone 3 | 24 | 50 | 0 | 0 | 0 | 3 | 8 | 38 | 1 | 0 | 0 | 0 |

| | | | numbers of chromosomes per metaphase | | | | | | | | | |
|---|---|---|---|---|---|---|---|---|---|---|---|---|
| **cell line:SW48 (stable ch-TOG knockdown)** | **percent of cells with a karyotype deviating from modal** | **metaphases analyzed** | **42** | **43** | **44** | **45** | **46** | **47** | **48** | **49** | **50** | **51** |
| SW48 + control shRNA, clone 1 | 30 | 50 | 0 | 0 | 0 | 2 | 8 | 35 | 5 | 0 | 0 | 0 |
| SW48 + control shRNA, clone 2 | 28 | 50 | 0 | 0 | 0 | 3 | 9 | 36 | 2 | 0 | 0 | 0 |
| SW48 + ch-TOG shRNA, clone 1 | 28 | 50 | 0 | 0 | 1 | 4 | 8 | 36 | 1 | 0 | 0 | 0 |
| SW48 + ch-TOG shRNA, clone 2 | 30 | 50 | 0 | 0 | 0 | 4 | 9 | 35 | 2 | 0 | 0 | 0 |
| SW48 + ch-TOG shRNA, clone 3 | 30 | 50 | 0 | 0 | 0 | 5 | 10 | 35 | 0 | 0 | 0 | 0 |

| | | | numbers of chromosomes per metaphase | | | | | | | | | |
|---|---|---|---|---|---|---|---|---|---|---|---|---|
| **cell line:SW837 (stable ch-TOG knockdown)** | **percent of cells with a karyotype deviating from modal** | **metaphases analyzed** | **35** | **36** | **37** | **38** | **39** | **40** | **41** | **42** | **47** | **48** |
| SW837 + control shRNA, clone 1 | 63 | 51 | 0 | 2 | 6 | 6 | 19 | 15 | 3 | 0 | 0 | 0 |
| SW837 + control shRNA, clone 2 | 56 | 50 | 0 | 0 | 6 | 8 | 22 | 8 | 5 | 1 | 0 | 0 |
| SW837 + ch-TOG shRNA, clone 1 | 36 | 50 | 0 | 0 | 4 | 8 | 32 | 6 | 0 | 0 | 0 | 0 |
| SW837 + ch-TOG shRNA, clone 2 | 26 | 50 | 0 | 0 | 4 | 37 | 5 | 4 | 0 | 0 | 0 | 0 |
| SW837 + ch-TOG shRNA, clone 3 | 28 | 50 | 0 | 0 | 5 | 4 | 36 | 3 | 2 | 0 | 0 | 0 |

| | | | numbers of chromosomes per metaphase | | | | | | | | | |
|---|---|---|---|---|---|---|---|---|---|---|---|---|
| **cell line:SW620 (stable ch-TOG knockdown)** | **percent of cells with a karyotype deviating from modal** | **metaphases analyzed** | **44** | **45** | **46** | **47** | **48** | **49** | **50** | **51** | **52** | **53** |
| SW620 + control shRNA, clone 1 | 58 | 60 | 0 | 0 | 0 | 6 | 11 | 25 | 11 | 5 | 1 | 1 |
| SW620 + control shRNA, clone 2 | 56 | 50 | 0 | 0 | 0 | 0 | 4 | 8 | 22 | 15 | 1 | 0 |
| SW620 + ch-TOG shRNA, clone 1 | 34 | 50 | 0 | 0 | 0 | 2 | 7 | 33 | 7 | 1 | 0 | 0 |
| SW620 + ch-TOG shRNA, clone 2 | 34 | 50 | 0 | 0 | 0 | 5 | 8 | 33 | 2 | 2 | 0 | 0 |
| SW620 + ch-TOG shRNA, clone 3 | 32 | 59 | 0 | 0 | 0 | 1 | 4 | 40 | 7 | 5 | 2 | 0 |

| | | | numbers of chromosomes per metaphase | | | | | | | | | |
|---|---|---|---|---|---|---|---|---|---|---|---|---|
| **cell line:SW480 (stable ch-TOG knockdown)** | **percent of cells with a karyotype deviating from modal** | **metaphases analyzed** | **52** | **53** | **54** | **55** | **56** | **57** | **58** | **59** | **60** | **61** |
| SW480 + control shRNA, clone 1 | 54 | 52 | 0 | 0 | 5 | 13 | 24 | 8 | 2 | 0 | 0 | 0 |
| SW480 + control shRNA, clone 2 | 64 | 50 | 0 | 0 | 4 | 5 | 18 | 13 | 10 | 0 | 0 | 0 |
| SW480 + ch-TOG shRNA, clone 1 | 36 | 50 | 0 | 0 | 0 | 5 | 5 | 32 | 7 | 1 | 0 | 0 |
| SW480 + ch-TOG shRNA, clone 2 | 28 | 50 | 0 | 0 | 1 | 2 | 9 | 36 | 2 | 0 | 0 | 0 |
| SW480 + ch-TOG shRNA, clone 3 | 32 | 50 | 0 | 0 | 2 | 3 | 34 | 11 | 0 | 0 | 0 | 0 |

**related to Figure 1f**

| | | | numbers of chromosomes per metaphase | | | | | | | | | |
|---|---|---|---|---|---|---|---|---|---|---|---|---|
| **cell line: HCT116 (Taxol treatment)** | **percent of cells with a karyotype deviating from modal** | **metaphases analyzed** | **41** | **42** | **43** | **44** | **45** | **46** | **47** | **48** | **49** | **50** |
| HCT116: DMSO (clone 1), see also Fig. 2c | 10 | 100 | 0 | 0 | 3 | 5 | 90 | 2 | 0 | 0 | 0 | 0 |
| HCT116: 0.5 nM Taxol (clone 1), see also Fig. 2c | 15 | 100 | 0 | 2 | 4 | 5 | 85 | 4 | 0 | 0 | 0 | 0 |

| | | | numbers of chromosomes per metaphase | | | | | | | | | |
|---|---|---|---|---|---|---|---|---|---|---|---|---|
| **cell line: SW837 (Taxol treatment)** | **percent of cells with a karyotype deviating from modal** | **metaphases analyzed** | **34** | **35** | **36** | **37** | **38** | **39** | **40** | **41** | **42** | **43** |
| SW837: DMSO, clone 1 | 50 | 105 | 0 | 2 | 2 | 10 | 52 | 31 | 8 | 0 | 0 | 0 |
| SW837: DMSO, clone 2 | 58 | 100 | 0 | 2 | 2 | 9 | 42 | 35 | 10 | 0 | 0 | 0 |
| SW837: + Taxol, clone 1 | 29 | 100 | 0 | 1 | 0 | 2 | 12 | 14 | 71 | 0 | 0 | 0 |
| SW837: + Taxol, clone 2 | 21 | 100 | 0 | 0 | 2 | 10 | 79 | 9 | 0 | 0 | 0 | 0 |
| SW837: + Taxol, clone 3 | 25 | 100 | 0 | 0 | 2 | 7 | 75 | 10 | 6 | 0 | 0 | 0 |
| SW837: clone 1 after Taxol removal | 58 | 100 | 0 | 0 | 2 | 10 | 16 | 22 | 42 | 8 | 0 | 0 |
| SW837: clone 2 after Taxol removal | 59 | 100 | 0 | 6 | 6 | 20 | 41 | 19 | 4 | 4 | 0 | 0 |
| SW837: clone 3 after Taxol removal | 57 | 100 | 0 | 4 | 6 | 10 | 43 | 27 | 6 | 4 | 0 | 0 |

| | | | numbers of chromosomes per metaphase | | | | | | | | | |
|---|---|---|---|---|---|---|---|---|---|---|---|---|
| **cell line: SW620 (Taxol treatment)** | **percent of cells with a karyotype deviating from modal** | **metaphases analyzed** | **44** | **45** | **46** | **47** | **48** | **49** | **50** | **51** | **52** | **53** |
| SW620: DMSOl, clone 1 | 52 | 100 | 0 | 0 | 4 | 13 | 20 | 48 | 12 | 3 | 0 | 0 |
| SW620: DMSO, clone 2 | 48 | 100 | 0 | 0 | 4 | 10 | 20 | 52 | 8 | 6 | 0 | 0 |
| SW620: + Taxol, clone 1 | 25 | 100 | 0 | 0 | 0 | 5 | 13 | 75 | 6 | 1 | 0 | 0 |
| SW620: + Taxol, clone 2 | 27 | 101 | 0 | 0 | 0 | 0 | 6 | 13 | 74 | 8 | 0 | 0 |
| SW620: + Taxol, clone 3 | 22 | 100 | 0 | 0 | 0 | 2 | 0 | 12 | 78 | 8 | 0 | 0 |
| SW620: clone 1 after Taxol removal | 54 | 100 | 0 | 0 | 4 | 6 | 18 | 46 | 22 | 4 | 0 | 0 |
| SW620: clone 2 after Taxol removal | 49 | 109 | 0 | 0 | 2 | 2 | 10 | 26 | 55 | 10 | 4 | 0 |
| SW620: clone 3 after Taxol removal | 51 | 100 | 0 | 0 | 2 | 8 | 8 | 24 | 49 | 9 | 0 | 0 |

| | | | numbers of chromosomes per metaphase | | | | | | | | | |
|---|---|---|---|---|---|---|---|---|---|---|---|---|
| **cell line: SW480 (Taxol treatment)** | **percent of cells with a karyotype deviating from modal** | **metaphases analyzed** | **52** | **53** | **54** | **55** | **56** | **57** | **58** | **59** | **60** | **61** |
| SW480: DMSO, clone 1 | 58 | 104 | 0 | 0 | 12 | 12 | 29 | 43 | 8 | 0 | 0 | 0 |
| SW480: DMSO, clone 2 | 59 | 100 | 0 | 0 | 8 | 16 | 41 | 32 | 3 | 0 | 0 | 0 |
| SW480: + Taxol, clone 1 | 27 | 100 | 0 | 0 | 4 | 5 | 14 | 73 | 4 | 0 | 0 | 0 |
| SW480: + Taxol, clone 2 | 27 | 100 | 0 | 0 | 2 | 4 | 15 | 73 | 6 | 0 | 0 | 0 |
| SW480: + Taxol, clone 3 | 26 | 100 | 0 | 0 | 4 | 8 | 74 | 8 | 6 | 0 | 0 | 0 |
| SW480: clone 1 after Taxol removal | 50 | 100 | 0 | 0 | 2 | 12 | 28 | 50 | 6 | 2 | 0 | 0 |
| SW480: clone 2 after Taxol removal | 58 | 100 | 0 | 0 | 8 | 10 | 30 | 42 | 6 | 2 | 2 | 0 |
| SW480: clone 3 after Taxol removal | 55 | 100 | 0 | 0 | 12 | 12 | 45 | 27 | 2 | 2 | 0 | 0 |

**related to Figure 1h**

| | | | numbers of chromosomes per metaphase | | | | | | | | | |
|---|---|---|---|---|---|---|---|---|---|---|---|---|
| **cell line: HCT116 (Nocodazol treatment)** | **percent of cells with a karyotype deviating from modal** | **metaphases analyzed** | **41** | **42** | **43** | **44** | **45** | **46** | **47** | **48** | **49** | **50** |
| HCT116: DMSOl, clone 1 | 16 | 50 | 0 | 0 | 0 | 6 | 42 | 2 | 0 | 0 | 0 | 0 |
| HCT116: DMSO, clone 2 | 16 | 50 | 0 | 0 | 0 | 7 | 42 | 1 | 0 | 0 | 0 | 0 |
| HCT116: + Nocodazol, clone 1 | 38 | 50 | 0 | 1 | 3 | 10 | 31 | 4 | 1 | 0 | 0 | 0 |
| HCT116: + Nocodazol, clone 2 | 36 | 50 | 0 | 0 | 1 | 8 | 32 | 9 | 0 | 0 | 0 | 0 |
| HCT116: + Nocodazol, clone 3 | 40 | 50 | 0 | 1 | 1 | 9 | 30 | 8 | 1 | 0 | 0 | 0 |

**related to Figure 2d**

| | | | numbers of chromosomes per metaphase | | | | | | | | | |
|---|---|---|---|---|---|---|---|---|---|---|---|---|
| **cell line: HCT116 (ch-TOG knockdown)** | **percent of cells with a karyotype deviating from modal** | **metaphases analyzed** | **41** | **42** | **43** | **44** | **45** | **46** | **47** | **48** | **49** | **50** |
| HCT116 + control shRNA | 12 | 50 | 0 | 0 | 0 | 4 | 44 | 2 | 0 | 0 | 0 | 0 |
| HCT116 + ch-TOG shRNA, clone 1 | 10 | 50 | 0 | 0 | 0 | 3 | 45 | 2 | 0 | 0 | 0 | 0 |
| HCT116 + ch-TOG shRNA, clone 2 | 8 | 50 | 0 | 0 | 0 | 3 | 46 | 1 | 0 | 0 | 0 | 0 |

| | | | numbers of chromosomes per metaphase | | | | | | | | | |
|---|---|---|---|---|---|---|---|---|---|---|---|---|
| **cell line: HCT116-CHK2-/- (ch-TOG knockdown)** | **percent of cells with a karyotype deviating from modal** | **metaphases analyzed** | **41** | **42** | **43** | **44** | **45** | **46** | **47** | **48** | **49** | **50** |
| HCT116-CHK2-/- + control shRNA | 48 | 50 | 0 | 0 | 6 | 26 | 13 | 5 | 0 | 0 | 0 | 0 |
| HCT116-CHK2-/- + ch-TOG shRNA, clone 1 | 20 | 50 | 0 | 0 | 6 | 40 | 4 | 0 | 0 | 0 | 0 | 0 |
| HCT116-CHK2-/- + ch-TOG shRNA, clone 2 | 24 | 50 | 0 | 0 | 1 | 7 | 38 | 3 | 1 | 0 | 0 | 0 |

**related to Figure 2g**

| | | | numbers of chromosomes per metaphase | | | | | | | | | |
|---|---|---|---|---|---|---|---|---|---|---|---|---|
| **cell line: HCT116 (Taxol, see also Fig. 1C)** | **percent of cells with a karyotype deviating from modal** | **metaphases analyzed** | **41** | **42** | **43** | **44** | **45** | **46** | **47** | **48** | **49** | **50** |
| HCT116: DMSO (see also Fig. 1C) | 9 | 101 | 0 | 0 | 2 | 4 | 91 | 4 | 0 | 0 | 0 | 0 |
| HCT116: 0.5 nM Taxol (see also Fig. 1C) | 10 | 101 | 0 | 0 | 1 | 7 | 91 | 2 | 0 | 0 | 0 | 0 |

| | | | numbers of chromosomes per metaphase | | | | | | | | | |
|---|---|---|---|---|---|---|---|---|---|---|---|---|
| **cell line: HCT116 + AURKA** | **percent of cells with a karyotype deviating from modal** | **metaphases analyzed** | **41** | **42** | **43** | **44** | **45** | **46** | **47** | **48** | **49** | **50** |
| HCT116+AURKA: DMSO, clone 1 | 42 | 103 | 0 | 4 | 14 | 18 | 60 | 7 | 0 | 0 | 0 | 0 |
| HCT116+AURKA: DMSO, clone 2 | 49 | 101 | 0 | 4 | 8 | 31 | 51 | 4 | 2 | 1 | 0 | 0 |
| HCT116+AURKA: + Taxol, clone 1 | 31 | 100 | 0 | 0 | 8 | 15 | 69 | 8 | 0 | 0 | 0 | 0 |
| HCT116+AURKA: + Taxol, clone 2 | 23 | 100 | 0 | 0 | 3 | 7 | 77 | 13 | 0 | 0 | 0 | 0 |
| HCT116+AURKA: + Taxol, clone 3 | 20 | 100 | 0 | 1 | 5 | 11 | 80 | 3 | 0 | 0 | 0 | 0 |
| HCT116+AURKA: clone 1 after Taxol removal | 48 | 100 | 0 | 4 | 6 | 14 | 52 | 22 | 2 | 0 | 0 | 0 |
| HCT116+AURKA: clone 2 after Taxol removal | 45 | 100 | 0 | 2 | 7 | 24 | 55 | 6 | 3 | 3 | 0 | 0 |
| HCT116+AURKA: clone 3 after Taxol removal | 46 | 100 | 0 | 2 | 10 | 20 | 54 | 12 | 2 | 0 | 0 | 0 |

| | | | numbers of chromosomes per metaphase | | | | | | | | | |
|---|---|---|---|---|---|---|---|---|---|---|---|---|
| **cell line: HCT116-CHK2-/-** | **percent of cells with a karyotype deviating from modal** | **metaphases analyzed** | **41** | **42** | **43** | **44** | **45** | **46** | **47** | **48** | **49** | **50** |
| HCT116-CHK2-/-: DMSO, clone 1 | 36 | 100 | 0 | 7 | 18 | 64 | 7 | 3 | 1 | 0 | 0 | 0 |
| HCT116-CHK2-/-: DMSO, clone 2 | 44 | 103 | 0 | 3 | 15 | 58 | 23 | 4 | 0 | 0 | 0 | 0 |
| HCT116-CHK2-/-: + Taxol, clone 1 | 25 | 102 | 0 | 0 | 6 | 76 | 16 | 3 | 0 | 1 | 0 | 0 |
| HCT116-CHK2-/-: + Taxol, clone 2 | 24 | 100 | 0 | 2 | 5 | 76 | 11 | 4 | 2 | 0 | 0 | 0 |
| HCT116-CHK2-/-: + Taxol, clone 3 | 18 | 100 | 0 | 0 | 0 | 82 | 13 | 5 | 0 | 0 | 0 | 0 |
| HCT116-CHK2-/-: clone 1 after Taxol removal | 46 | 100 | 0 | 2 | 10 | 54 | 26 | 8 | 0 | 0 | 0 | 0 |
| HCT116-CHK2-/-: clone 2 after Taxol removal | 61 | 100 | 0 | 4 | 7 | 39 | 30 | 14 | 4 | 2 | 0 | 0 |
| HCT116-CHK2-/-: clone 3 after Taxol removal | 52 | 109 | 0 | 5 | 11 | 52 | 32 | 8 | 1 | 0 | 0 | 0 |

**related to Figure 6e**

| | | | numbers of chromosomes per metaphase | | | | | | | | | |
|---|---|---|---|---|---|---|---|---|---|---|---|---|
| **cell line: HCT116-CHK2-/- (AURKA knockdown)** | **percent of cells with a karyotype deviating from modal** | **metaphases analyzed** | **40** | **41** | **42** | **43** | **44** | **45** | **46** | **47** | **48** | **49** |
| HCT116-CHK2-/- + control shRNA | 37 | 91 | 0 | 0 | 0 | 23 | 63 | 5 | 0 | 0 | 0 | 0 |
| HCT116-CHK2-/- + AURKA shRNA, clone 1 | 11 | 98 | 0 | 0 | 0 | 6 | 89 | 3 | 0 | 0 | 0 | 0 |
| HCT116-CHK2-/- + AURKA shRNA, clone 2 | 14 | 98 | 0 | 0 | 0 | 6 | 87 | 5 | 0 | 0 | 0 | 0 |
| HCT116-CHK2-/- + AURKA shRNA, clone 3 | 13 | 100 | 0 | 0 | 0 | 8 | 89 | 2 | 0 | 0 | 0 | 0 |

**related to Figure 6g**

| | | | numbers of chromosomes per metaphase | | | | | | | | | |
|---|---|---|---|---|---|---|---|---|---|---|---|---|
| **cell line: SW48 (AURKA knockdown)** | **percent of cells with a karyotype deviating from modal** | **metaphases analyzed** | **43** | **44** | **45** | **46** | **47** | **48** | **49** | **50** | **51** | **52** |
| SW48 + control shRNA | 14 | 100 | 0 | 0 | 1 | 6 | 86 | 5 | 2 | 0 | 0 | 0 |
| SW48 + AURKA shRNA, clone 1 | 14 | 100 | 0 | 0 | 3 | 8 | 86 | 3 | 0 | 0 | 0 | 0 |

| | | | numbers of chromosomes per metaphase | | | | | | | | | |
|---|---|---|---|---|---|---|---|---|---|---|---|---|
| **cell line: RKO (AURKA knockdown)** | **percent of cells with a karyotype deviating from modal** | **metaphases analyzed** | **44** | **45** | **46** | **47** | **48** | **49** | **50** | **51** | **52** | **53** |
| RKO + control shRNA | 17 | 100 | 0 | 1 | 1 | 10 | 83 | 5 | 0 | 0 | 0 | 0 |
| RKO + AURKA shRNA, clone 1 | 25 | 100 | 0 | 1 | 4 | 12 | 75 | 8 | 0 | 0 | 0 | 0 |
| RKO + AURKA shRNA, clone 2 | 16 | 104 | 0 | 0 | 0 | 2 | 12 | 87 | 3 | 0 | 0 | 0 |
| RKO + AURKA shRNA, clone 3 | 18 | 100 | 0 | 0 | 5 | 9 | 82 | 4 | 0 | 0 | 0 | 0 |

| | | | numbers of chromosomes per metaphase | | | | | | | | | |
|---|---|---|---|---|---|---|---|---|---|---|---|---|
| **cell line: SW837 (AURKA knockdown)** | **percent of cells with a karyotype deviating from modal** | **metaphases analyzed** | **35** | **36** | **37** | **38** | **39** | **40** | **41** | **42** | **43** | **44** |
| SW837 + control shRNA | 51 | 100 | 0 | 3 | 4 | 7 | 49 | 32 | 2 | 3 | 0 | 0 |
| SW837 + AURKA shRNA, clone 1 | 34 | 81 | 0 | 2 | 3 | 9 | 8 | 53 | 4 | 1 | 0 | 1 |

| | | | numbers of chromosomes per metaphase | | | | | | | | | |
|---|---|---|---|---|---|---|---|---|---|---|---|---|
| **cell line: SW620 (AURKA knockdown)** | **percent of cells with a karyotype deviating from modal** | **metaphases analyzed** | **44** | **45** | **46** | **47** | **48** | **49** | **50** | **51** | **52** | **53** |
| SW620 + control shRNA | 51 | 100 | 0 | 0 | 2 | 4 | 17 | 49 | 25 | 3 | 0 | 0 |
| SW620 + AURKA shRNA, clone 1 | 33 | 100 | 0 | 0 | 0 | 0 | 3 | 6 | 18 | 67 | 6 | 0 |
| SW620 + AURKA shRNA, clone 2 | 23 | 100 | 0 | 0 | 0 | 0 | 0 | 6 | 13 | 77 | 4 | 0 |
| SW620 + AURKA shRNA, clone 3 | 28 | 100 | 0 | 0 | 0 | 0 | 1 | 3 | 16 | 72 | 8 | 0 |

| | | | numbers of chromosomes per metaphase | | | | | | | | | |
|---|---|---|---|---|---|---|---|---|---|---|---|---|
| **cell line: SW480 (AURKA knockdown)** | **percent of cells with a karyotype deviating from modal** | **metaphases analyzed** | **51** | **52** | **53** | **54** | **55** | **56** | **57** | **58** | **59** | **60** |
| SW480 + control shRNA | 47 | 100 | 0 | 1 | 1 | 7 | 9 | 20 | 53 | 8 | 1 | 0 |
| SW480 + AURKA shRNA, clone 1 | 27 | 100 | 0 | 1 | 2 | 2 | 5 | 14 | 73 | 3 | 0 | 0 |

**related to Supplementary Figure S2e**

| | | | numbers of chromosomes per metaphase | | | | | | | | | |
|---|---|---|---|---|---|---|---|---|---|---|---|---|
| **cell line: HCT116 (AURKA overexpression)** | **percent of cells with a karyotype deviating from modal** | **metaphases analyzed** | **41** | **42** | **43** | **44** | **45** | **46** | **47** | **48** | **49** | **50** |
| HCT116 + control vector | 11 | 100 | 0 | 0 | 2 | 9 | 89 | 0 | 0 | 0 | 0 | 0 |
| HCT116 + AURKA, clone 1 | 33 | 101 | 0 | 3 | 6 | 20 | 68 | 4 | 0 | 0 | 0 | 0 |
| HCT116 + AURKA, clone 2 | 31 | 102 | 0 | 4 | 10 | 14 | 70 | 4 | 0 | 0 | 0 | 0 |
| HCT116 + AURKA, clone 3 | 28 | 100 | 0 | 1 | 7 | 15 | 72 | 5 | 0 | 0 | 0 | 0 |

**related to Suppementary Figure S8i**

| | | | numbers of chromosomes per metaphase | | | | | | | | | |
|---|---|---|---|---|---|---|---|---|---|---|---|---|
| **cell line: SW620 (Xenograft re-isolation)** | **percent of cells with a karyotype deviating from modal** | **metaphases analyzed** | **44** | **45** | **46** | **47** | **48** | **49** | **50** | **51** | **52** | **53** |
| mouse #1: SW620 + control shRNA | 54 | 50 | 0 | 0 | 2 | 7 | 11 | 23 | 5 | 2 | 0 | 0 |
| mouse #1: SW620 + AURKA shRNA | 24 | 50 | 0 | 0 | 0 | 1 | 1 | 10 | 38 | 0 | 0 | 0 |
| mouse #2: SW620 + control shRNA | 56 | 50 | 0 | 0 | 1 | 5 | 18 | 22 | 4 | 0 | 0 | 0 |
| mouse #2: SW620 + AURKA shRNA | 32 | 50 | 0 | 0 | 0 | 0 | 0 | 2 | 13 | 34 | 0 | 1 |
| mouse #3: SW620 + control shRNA | 44 | 50 | 0 | 0 | 2 | 4 | 9 | 28 | 6 | 1 | 0 | 0 |
| mouse #3: SW620 + AURKA shRNA | 22 | 50 | 0 | 0 | 0 | 0 | 0 | 3 | 5 | 39 | 3 | 0 |